



UNIVERSITY OF LEEDS

This is a repository copy of *Structural insight into the formation of lipoprotein- β -barrel complexes*.

White Rose Research Online URL for this paper:
<http://eprints.whiterose.ac.uk/160995/>

Version: Accepted Version

Article:

Rodríguez-Alonso, R, Létoquart, J, Nguyen, VS et al. (7 more authors) (2020) Structural insight into the formation of lipoprotein- β -barrel complexes. *Nature Chemical Biology*. ISSN 1552-4450

<https://doi.org/10.1038/s41589-020-0575-0>

© 2020, Springer Nature. This is an author produced version of an article published in *Nature Chemical Biology*. Uploaded in accordance with the publisher's self-archiving policy.

Reuse

Items deposited in White Rose Research Online are protected by copyright, with all rights reserved unless indicated otherwise. They may be downloaded and/or printed for private study, or other acts as permitted by national copyright laws. The publisher or other rights holders may allow further reproduction and re-use of the full text version. This is indicated by the licence information on the White Rose Research Online record for the item.

Takedown

If you consider content in White Rose Research Online to be in breach of UK law, please notify us by emailing eprints@whiterose.ac.uk including the URL of the record and the reason for the withdrawal request.



eprints@whiterose.ac.uk
<https://eprints.whiterose.ac.uk/>

1 **Structural insight into the formation of lipoprotein- β -barrel complexes**

2

3 **Raquel Rodríguez-Alonso^{1,2,7}, Juliette Létoquart^{1,2,7}, Van Son Nguyen^{3,4}, Gwennaëlle**
4 **Louis^{1,2}, Antonio N. Calabrese⁵, Bogdan I. Iorga⁶, Sheena E. Radford⁵, Seung-Hyun**
5 **Cho^{1,2,*}, Han Remaut^{3,4,*} and Jean-François Collet^{1,2,*}**

6

7 ¹WELBIO - Walloon Excellence in Life Sciences and Biotechnology, Avenue Hippocrate 75,
8 1200 Brussels, Belgium

9 ²de Duve Institute, Université catholique de Louvain, Avenue Hippocrate 75, 1200 Brussels,
10 Belgium

11 ³Structural Biology Brussels, Vrije Universiteit Brussel, 1050 Brussels, Belgium

12 ⁴Structural and Molecular Microbiology, Structural Biology Research Center, VIB, 1050
13 Brussels, Belgium

14 ⁵Astbury Centre for Structural Molecular Biology, School of Molecular and Cellular Biology,
15 Faculty of Biological Sciences, University of Leeds, Leeds LS2 9JT, UK

16 ⁶Université Paris-Saclay, CNRS UPR 2301, Institut de Chimie des Substances Naturelles,
17 91198 Gif-sur-Yvette, France

18 ⁷co-first authors

19 *Correspondence: seung.cho@uclouvain.be, han.remaut@vub.be, and jfcollet@uclouvain.be

20

21 **The β -barrel assembly machinery (BAM) inserts outer membrane β -barrel proteins**
22 **(OMPs) in the outer membrane of Gram-negative bacteria. In Enterobacteriaceae, BAM**
23 **also mediates export of the stress sensor lipoprotein RcsF to the cell surface by assembling**
24 **RcsF-OMP complexes. Here, we report the crystal structure of the key BAM component**
25 **BamA in complex with RcsF. BamA adopts an inward-open conformation, with the**

26 lateral gate to the membrane closed. RcsF is lodged deep inside the lumen of the BamA
27 barrel, binding regions proposed to undergo an outward and lateral opening during OMP
28 insertion. On the basis of our structural and biochemical data, we propose a push-and-
29 pull model for RcsF export upon conformational cycling of BamA and provide a
30 mechanistic explanation for how RcsF uses its interaction with BamA to detect envelope
31 stress. Our data also suggest that the flux of incoming OMP substrates is involved in the
32 control of BAM activity.

33

34 Introduction

35

36 The vast majority of proteins inserted in the outer membrane of Gram-negative bacteria adopt
37 a β -barrel conformation. Their assembly depends on the activity of the conserved β -barrel
38 assembly machinery (BAM), whose core component is the OMP85-family protein BamA^{1,2}.
39 BamA is an outer membrane 16-stranded β -barrel with a large periplasmic extension consisting
40 of five POlypeptide TRansport-Associated (POTRA) domains at its N-terminus¹. Structures
41 of BAM have shown that BamA can adopt two conformations: an outward-open conformation
42^{3,4}, in which the β -barrel domain opens between strands β 1 and β 16 to form a lateral gate to the
43 membrane, and an inward-open conformation^{5,6}, in which the lateral gate is sealed while a
44 periplasmic entry pore to the barrel lumen is open. In the bacterium *Escherichia coli*, four
45 accessory lipoproteins (BamB, BamC, BamD, and BamE) complete BAM, forming a
46 pentameric holocomplex^{7,8}. BamBCDE are anchored to the outer membrane by a lipid moiety
47 but reside in the periplasm. BamB and BamD directly bind the POTRA domains of BamA,
48 while BamC and BamE bind BamD^{1,2}. Although all components are required for efficient
49 assembly of *E. coli*'s diverse set of OMPs, only BamA and BamD are essential and conserved
50 throughout Gram-negative bacteria^{1,2}. Despite important structural and functional insights

51 during 15 years of intense scrutiny due to the essential activity of BAM in generating and
52 maintaining the outer membrane, crucial questions remain unsolved regarding the mechanism
53 of this molecular machine. In particular, the functional importance of BamA cycling between
54 the outward-open and inward-open conformations remains unclear, as are the respective
55 contributions of the various BAM components to OMP assembly ⁹.

56

57 The primary function of BAM is the assembly of OMPs and, when necessary, the translocation
58 of their associated extracellular domains across the outer membrane. More recently, BAM has
59 also been implicated in export of the outer membrane lipoprotein RcsF to the cell surface ^{10,11}
60 via the assembly of complexes between this lipoprotein and three abundant OMPs (OmpA,
61 OmpC, and OmpF) ^{10,11}. Support for the involvement of BAM in RcsF export comes from *in*
62 *vivo* crosslinking experiments in which a complex between RcsF and BamA, considered to be
63 an intermediate in the formation of RcsF-OmpA/C/F complexes, was trapped ^{10,11}. Further, in
64 cells lacking BamB and BamE, RcsF accumulates on BamA and causes a lethal block to BAM-
65 mediated OMP assembly, suggesting that OMPs and surface-exposed RcsF exploit at least
66 partially overlapping assembly routes ^{12,13}.

67

68 RcsF functions as an envelope stress sensor capable of mounting a protective response when
69 damage occurs in the peptidoglycan or in the outer membrane ^{14,15}. Interestingly, we previously
70 determined that sending RcsF to the surface is part of a cellular strategy that enables RcsF to
71 detect damage in the cell envelope. Under stress conditions, newly synthesized RcsF molecules
72 fail to interact with BamA ¹⁰: they are not exported to the surface and remain exposed to the
73 periplasm, which allows them to trigger the Rcs signaling cascade by reaching the downstream
74 Rcs partner in the inner membrane ¹⁶. Thus, surface exposure is intimately linked to the
75 function of RcsF. However, the molecular details of the BamA-RcsF interaction, how BAM

76 orchestrates the export of RcsF with OMP assembly, and what prevents RcsF from interacting
77 with BamA under stress conditions remain unknown. Here we sought to address these
78 questions by obtaining structural information about the interaction between BamA and RcsF.

79

80 **Results**

81

82 **RcsF can be purified with the BAM complex**

83 In a series of exploratory experiments, we co-overexpressed RcsF with the BamAB sub-
84 complex, or with the BamABCDE holocomplex; both BamAB-RcsF and BamABCDE-RcsF
85 could be detergent-extracted from the membrane and purified via affinity chromatography
86 using a His-tag on the N-terminus of BamA (Fig. 1a). Using native gel electrophoresis, we
87 confirmed that RcsF binds BamABCDE, and not only BamAB (Fig. 1a, b, c). However,
88 whereas BamAB-RcsF was stable and could be purified to homogeneity by size-exclusion
89 chromatography, BamABCDE-RcsF was unstable (Extended Data Fig. 1a, b). Interesting to
90 note, destabilization of BamABCDE was only observed when RcsF was present (Extended
91 Data Fig. 1c).

92

93 **BamA is in the inward-open conformation in the structure**

94 The BamAB-RcsF complex was crystallized and its structure solved to 3.8 Å resolution by
95 molecular replacement using the structures of BamA and RcsF (PDB: 5D0O and 2Y1B,
96 respectively; Supplementary Table 1). While this structure contained BamA and RcsF (Fig. 2),
97 BamB dissociated from the BamA-RcsF complex during crystallization and was absent. The
98 asymmetric unit contained two BamA-RcsF conformers, although for one of them, no
99 unambiguous electron density was observed for POTRA domains 1, 2, 3, and 5 (Extended Data
100 Fig. 2a, b). The β -barrel of BamA was found in an inward-open conformation closely matching

101 that reported in structures of *E. coli* BamABCDE (⁶, with a root mean square deviation of 0.9
102 Å for 383 equivalent C α atoms in the BamA β -barrel of PDB: 5D0O) or BamA truncates
103 lacking POTRA domains 1-4 or 1-5 ¹⁷⁻²⁰.

104

105 **RcsF is located inside the lumen of the BamA β -barrel**

106 In both BamA copies, RcsF was lodged deep inside the lumen of the BamA β -barrel (Fig. 2a;
107 Extended Data Fig. 2c). RcsF contacts two BamA loops protruding into the β -barrel: (1)
108 extracellular loop L6 (^eL6; ~77 Å² buried surface area, one putative H bond; note that at 3.8 Å
109 resolution, amino-acid sidechain positions cannot be unambiguously determined), and (2) the
110 periplasmic loop connecting strands 7 and 8 (^pL4; ~140 Å² buried surface area, one putative H
111 bond) (Fig. 2, 3a). Although contacting RcsF, these loops retain a conformation closely
112 matching that seen in inward-open BamA structures (Fig. 3b). However, the main BamA-RcsF
113 contact occurs through the luminal wall of the BamA β -barrel, encompassing ~1100 Å² of
114 buried surface area and comprising up to 15 putative H-bonds (Fig. 2). This RcsF-BamA β -
115 barrel interaction can be divided into three zones. Zone 1 (Z1) consists of perhaps nine H bonds
116 formed by BamA residue 488 and residues 463, 465, and 466 in the loop connecting β 3 and β 4
117 and contacting the RcsF loop connecting β 1 and α 1 (L ^{β 1- α 1}) (Fig. 2b, c, Fig. 3a, c). Zone 2 (Z2)
118 is made of perhaps four H bonds formed by BamA residues 592 and 634, located above ^pL4
119 (Fig. 2c, 3a). β 16, one of the components of the proposed lateral gate of the BamA β -barrel,
120 constitutes the third zone (Fig. 2b, c, 3a). The bottom of RcsF protrudes out of the BamA β -
121 barrel into the periplasm, residing in close proximity to POTRA domains 3-5 (Fig. 2a, b). As
122 a result, RcsF sterically pushes POTRA5 outward, causing a 26° rotation compared to the
123 inward-open conformation found in BamA structures ^{5,6} (Fig. 3b). Although the lipid anchor
124 of RcsF and the N-terminal disordered linker (residues 16-50) ^{21,22} are not apparent in this
125 structure, the position of RcsF is compatible with the lipid anchor residing in the inner leaflet

126 of the outer membrane. Of note, the binding interface between RcsF and BamA does not
127 overlap with the binding sites of BamA for its accessory lipoproteins (Extended Data Fig. 3).
128 Consistent with this observation, the RcsF-BamA interaction is compatible with the binding of
129 BamBCDE, as determined experimentally (Fig. 1; Extended Data Fig. 1).
130
131 To validate the BamA-RcsF conformation revealed by the X-ray structure, we subjected the
132 complex to crosslinking and analysis via mass spectrometry using the homobifunctional NHS-
133 ester crosslinker disuccinimidyl dibutyric urea ²³. The sequence coverage of RcsF was about
134 60% (Extended Data Fig. 4a). Note that one peptide from the N-terminal linker was detected,
135 indicating that the N-terminal disordered region was not degraded during purification.
136 Crosslinks were identified between lysine residues in RcsF (two lysines from the globular
137 domain and one located at the C-terminus of the linker) and those in POTRA4 and POTRA5
138 (Extended Data Fig. 4b; Supplementary Table 2), providing further support for the architecture
139 of BamA-RcsF determined by crystallography. To confirm that RcsF binds inside the barrel of
140 BamA, we incorporated the photoreactive lysine analog N6-((3-(3-methyl-3H-diazirin-3-
141 yl)propyl)carbamoyl)-L-lysine (DiZPK) ²⁴ at multiple positions in the BamA β -barrel domain,
142 selecting residues (R583, R592, K598, K610, R632, R634, R661, K808) whose sidechains face
143 the lumen of the barrel (Extended Data Fig. 4b). After exposure to ultraviolet light, RcsF
144 efficiently crosslinked to BamA when DiZPK was incorporated at three of the selected residues
145 (R592, R598, K610) and to a lower extent at residue K808 (Extended Data Fig. 4b, c),
146 confirming that RcsF binds deep inside the barrel. We measured an equilibrium dissociation
147 constant of 350 \pm 49 or 420 \pm 48 nM, respectively, depending on whether BamA or RcsF was
148 immobilized (Extended Data Fig. 4d, e). Finally, we deleted loop 1, a short, non-essential ²⁵
149 segment located between the first and second β -strands of the barrel (residues 434 to 437;
150 BamA $_{\Delta$ loop1) (Fig. 3a; Extended Data Fig. 4b). BamA $_{\Delta$ loop1 is functional ⁵ and able to rescue the

151 lethality of a $\Delta bamA$ deletion mutant, despite the fact that the levels of major OMPs are slightly
152 decreased in cells expressing BamA $_{\Delta loop1}$ (Extended Data Fig. 4f). We hypothesized that
153 deleting this loop would destabilize the BamA-RcsF interaction because of the close proximity
154 of loop 1 to the lateral gate area and to loop 6, two regions of interaction between BamA and
155 RcsF. As predicted, RcsF could be pulled down with BamA but not with BamA $_{\Delta loop1}$ (Extended
156 Data Fig. 4g). Further, the Rcs signaling cascade, which is turned on when RcsF fails to interact
157 with BamA¹⁰, was constitutively induced in $\Delta bamA$ cells complemented with BamA $_{\Delta loop1}$
158 (Extended Data Fig. 4h). In sum, these results provide functional evidence for our structure of
159 BamA-RcsF and confirm the presence of RcsF inside the barrel of BamA.

160

161 **RcsF does not bind BamA when the lateral gate is open**

162 Strikingly, our structure suggests that RcsF binding is incompatible with the BamA β -barrel
163 residing in the outward-open conformation (Fig. 3a). Confirming this hypothesis, RcsF was
164 found to bind BamA^{G433C/N805C}, a mutant in which opening of the lateral gate is prevented by a
165 disulfide bond between $\beta 1$ and $\beta 16$ ²⁶, but not to BamA^{G393C/G584C}, which is locked in the
166 outward-open conformation⁵ (Extended Data Fig. 5a, b). However, when reduced,
167 BamA^{G393C/G584C} returned to the inward-open conformation and regained the ability to bind
168 RcsF (Extended Data Fig. 5c). Importantly, given its ability to only bind the inward-open
169 conformation of BamA, the BamA-RcsF complex serves as a proxy for this state. Interestingly,
170 RcsF was recently reported to accumulate on BamA and to jam OMP assembly in the absence
171 of BamB and BamE^{12,13}. Thus, in light of our structural findings, BamA conformational
172 cycling is likely impaired when BamB and BamE are absent. However, binding of these
173 accessory lipoproteins cannot be sufficient to trigger conformational changes in BamA. The
174 structure of BamABCDE has been solved not only in the outward-open conformation but also
175 in the inward-open conformation³⁻⁶, despite the presence of all accessory lipoproteins. In

176 addition, we have shown here that RcsF could be co-purified with BamABCDE (Fig. 1;
177 Extended Data Fig. 1), implying that in this purified complex, BamA was in the inward-open
178 conformation. Thus, BamA can remain in the inward-open conformation even when
179 BamBCDE are present, strongly supporting the notion that BAM conformational cycling is
180 triggered by an external signal.

181

182 **OMP substrates trigger conformational cycling in BamA**

183 What is this trigger? Insights came from *in vivo* crosslinking experiments carried out in cells
184 in which the expression levels of the BAM components were only moderately increased (~2-
185 fold) compared with wild-type levels. Whereas RcsF can be crosslinked to BamA when the
186 BamA and BamB subunits are slightly over-expressed, the BamA-RcsF complex becomes
187 barely detectable when the moderate over-expression of all BAM components is induced (Fig.
188 4 a, b). We explain this as follows: the BamAB subcomplex is not functional and does not
189 funnel RcsF to its OMP partners. As a result, BamA-RcsF accumulates and OmpA-RcsF does
190 not form (Fig. 4a). However, if all BAM components (BamABCDE) are moderately
191 overexpressed, BAM activity is restored, RcsF only transiently interacts with BamA, and
192 formation of OmpA-RcsF resumes (Fig. 4a; note that in these experiments, BAM is still
193 expressed at physiological levels from the chromosome—by using plasmids, we manipulate
194 the stoichiometry of the BAM components (Fig. 4b)). Therefore, whether a stable RcsF
195 complex forms with BAM depends critically on the rates of OMP synthesis and delivery to
196 BAM, as well as the ratio of active BAM complexes to the concentrations of OMP and RcsF
197 substrates. When we purified the BamABCDE-RcsF complex (Fig. 1; Extended Data Fig. 1),
198 all BAM components were highly over-expressed, which increased the ratio of active
199 complexes to incoming OMP substrates and allowed accumulation of RcsF on BAM. Thus,
200 our data support a model in which it is the flux of incoming OMP substrates that triggers

201 conformational changes in the BamA barrel and release of RcsF to its OMP partners (see
202 below; Fig. 4c). Although complexes have to date only been observed between RcsF and
203 OmpA/C/F^{10,11}, complexes may form between RcsF and other, less abundant OMPs,
204 depending on the unfolded OMP that is delivered to the BamABCDE-RcsF complex.

205

206 **RcsF is transferred to its partners during BamA cycling**

207 RcsF is not an integral component of BAM; it can bind BamA with high affinity, but it is
208 eventually funneled to OMPs and displayed on the cell surface^{10,11}. It has been proposed that
209 RcsF crosses the outer membrane by being threaded through the lumens of OMPs¹¹. In one
210 possible scenario, RcsF could be transferred from BamA to its OMP partner following opening
211 of the lateral gate and formation of a hybrid barrel (or another non-covalent complex⁹ between
212 BamA and the nascent OMP), which then buds away from BamA, taking RcsF with it.
213 Available structures show that the transition from the inward-open to the outward-open
214 conformation of BamA encompasses a large outward rotation of strands 1-6 of the BamA β -
215 barrel, as well as a 20 Å inward displacement of POTRA 5 (Fig. 3a, b, c)^{5,6}. Strikingly, BamA
216 strands 1-6 coincide with the main RcsF-BamA interaction zone (Z1) seen in our structure,
217 such that outward rotation of Z1 may exert a pulling force on the tip of RcsF (Fig. 3a, c).
218 Concomitantly, the inward movement of POTRA5 would exert a pushing force on the bottom
219 of RcsF (Fig. 3c). We therefore hypothesize that during the inward-to-outward transition of
220 BamA, this push-and-pull action on RcsF could play a role in the transfer of RcsF to its OMP
221 partners and its translocation to the cell surface (Fig. 4c). Supporting this, dynamic importance
222 sampling simulations in which BamA transitions from the inward-open conformation (as in
223 our structure) to the outward-open conformation (PDB code 5D0Q) show POTRA5 moving
224 towards the periplasmic exit of the lumen, pushing RcsF upwards. The movement of POTRA5
225 is accompanied later on by the movement of Z1, opening the outward-facing extremity

226 (Extended Data Fig. 6a, b, c, d and Supplementary Video). Furthermore, by introducing a short
227 peptide in the hinge between POTRA5 and the β -barrel domain of BamA (BamA^{hinge}), we
228 could confirm the functional importance of this region for BamA activity. We found indeed
229 that expression of BamA^{hinge} from a plasmid rescues the growth of $\Delta bamA$ cells in minimal
230 media at 30°C but not in rich media at 37°C, indicating that BamA^{hinge} is unable to cope with
231 the rate of OMPs folding in these latter conditions (Extended Data Fig. 6e).

232

233 **Discussion**

234

235 Our work reveals how BamA interacts with RcsF, providing insights into the mechanism used
236 by BAM to assemble RcsF-OMP complexes, a novel activity by which BAM exports this
237 lipoprotein to the cell surface. It would be surprising if an essential machinery such as BAM—
238 with a global role in formation of the cell envelope—was only dedicated to export RcsF to the
239 surface. Hence, it is tempting to speculate that other lipoproteins may follow the same route
240 and decorate the surface of *E. coli*, in contrast to the general view that outer membrane
241 lipoproteins face the periplasm²⁷.

242

243 By showing that the globular domain of RcsF is lodged deep inside the barrel of BamA, our
244 structure also reveals the remarkable—and unanticipated—finding that the BamA β -barrel can
245 accommodate a lipoprotein “substrate” with a globular domain 12 kDa in size. This finding
246 further establishes BAM as an essential hub that contributes to outer membrane biogenesis by
247 interacting both with nascent OMPs for assembly and lipoproteins for export. Future work will
248 reveal whether other lipoproteins bind BamA in a way similar to RcsF and also clarify the
249 topology of the RcsF-OMP complexes. It has indeed been proposed that the lipid moiety of
250 RcsF is anchored in the outer leaflet of the membrane and that the N-terminal disordered linker

251 is exposed on the cell surface before being threaded through the lumens of the OMPs ¹¹. In this
252 model, the globular domain of RcsF resides inside the periplasm. Although we cannot rule out
253 that RcsF flips during release from BamA and transfer to its OMP partners, our structure is
254 more consistent with the hypothesis that BamA releases the globular domain of RcsF on the
255 cell surface. Further investigation will therefore be needed to answer this question, and whether
256 the location of RcsF depends on the identity of its OMP partner.

257

258 It is also remarkable that RcsF binds the lateral gate area and the outward rotating region of the
259 BamA barrel, sites that sense BAM conformational cycling triggered by incoming OMP
260 substrates. We previously reported that RcsF uses its interaction with BamA to detect stress in
261 the cell envelope: when damage occurs in the peptidoglycan or the outer membrane, newly
262 synthesized RcsF molecules fail to interact with BamA, activating the Rcs stress response ¹⁰.
263 Our structure provides a possible explanation for this scenario by suggesting that BamA
264 preferentially adopts the outward-open conformation when envelope integrity is impaired,
265 which would *de facto* prevent RcsF binding and promote Rcs activation. Thus, we propose that
266 cells could monitor envelope integrity via the conformational cycling of BamA.

267

268 How the outer membrane of Gram-negative bacteria is assembled remains a long-standing
269 mystery and a crucial question in biology. Here, we focused on BamA, the core component of
270 BAM whose activity is essential to constructing and maintaining the outer membrane. By
271 solving the structure of BamA in complex with its lipoprotein substrate RcsF, our work sheds
272 new light on BAM. It not only provides crucial molecular insights into how BAM exports
273 lipoproteins to the surface, but also uncovers important new features of this essential machinery
274 and its mechanism. Because BAM activity is required for bacterial survival, the complex is an
275 attractive target for new antibiotics ²⁸⁻³¹. Our work also paves the way to the design of new

276 antibacterials that interfere with BAM conformational cycling, because blocking BAM in the
277 inward-open conformation lethally jams BAM with RcsF.

278

279 **ACKNOWLEDGMENTS**

280 We thank Asma Boujtat for technical help. We are indebted to Dr. Peng R. Chen (Peking
281 University) for sharing DiZPK, to Dr. Harris Bernstein (NIH, Bethesda, USA) for providing
282 strains and plasmids, and to Dr. Michael Deghelt, Dr. Géraldine Laloux, Dr. Camille Goemans
283 (EMBL, Heidelberg, Germany), and Dr. Pauline Leverrier for helpful suggestions and
284 discussions and for providing comments on the manuscript. We thank Pierre Legrand and staff
285 at Soleil Synchrotron France and at Diamond Light Source UK for beamtime and their
286 assistance during data collection. This work was supported, in part, by grants from the Fonds
287 de la Recherche Scientifique – FNRS, from the FRFS-WELBIO grants n° WELBIO-CR-
288 2015A-03 and WELBIO-CR-2019C-03, from the EOS Excellence in Research Program of the
289 FWO and FRS-FNRS (G0G0818N), from the Fédération Wallonie-Bruxelles (ARC 17/22-
290 087), from the European Commission via the International Training Network Train2Target
291 (721484), from the French region Ile-de-France (DIM Malinf) and from the BBSRC
292 (BB/P000037/1, BB/M012573/1).

293

294 **AUTHOR CONTRIBUTIONS**

295 J.-F.C., R.R.A., S.E.R., H.R., and S.H.C. wrote the manuscript. J.L., RRA, S.N., G.L., S.H.C.,
296 H.R., and J.-F.C. designed the experiments. J.L., R.R.A., S.N., G.L., and S.H.C. performed the
297 experiments, constructed the strains, and cloned the constructs. B.I. performed the dynamic
298 importance sampling simulations. J.L., R.R.A., S.N., S.H.C., H.R., and J.-F.C. analyzed and
299 interpreted the data. A.N.C. and S.E.R. performed and analyzed the crosslinking mass
300 spectrometry experiments. All authors discussed the results and commented on the manuscript.

301

302 AUTHOR INFORMATION

303 The authors declare no competing financial interests.

304

305 DATA AVAILABILITY

306 Coordinates and structure factors have been deposited in the Protein Data Bank under accession
307 number 6T1W. All other data generated or analysed during this study are included in this
308 published article and its supplementary information file.

309

310 REFERENCES

311 1 Noinaj, N., Gumbart, J. C. & Buchanan, S. K. The beta-barrel assembly machinery in
312 motion. *Nat Rev Microbiol* **15**, 197-204, doi:10.1038/nrmicro.2016.191 (2017).

313 2 Hagan, C. L., Silhavy, T. J. & Kahne, D. beta-Barrel membrane protein assembly by
314 the Bam complex. *Annu Rev Biochem* **80**, 189-210, doi:10.1146/annurev-biochem-
315 061408-144611 (2011).

316 3 Iadanza, M. G. *et al.* Lateral opening in the intact beta-barrel assembly machinery
317 captured by cryo-EM. *Nat Commun* **7**, 12865, doi:10.1038/ncomms12865 (2016).

318 4 Bakelar, J., Buchanan, S. K. & Noinaj, N. The structure of the beta-barrel assembly
319 machinery complex. *Science* **351**, 180-186, doi:10.1126/science.aad3460 (2016).

320 5 Gu, Y. *et al.* Structural basis of outer membrane protein insertion by the BAM complex.
321 *Nature* **531**, 64-69, doi:10.1038/nature17199 (2016).

322 6 Han, L. *et al.* Structure of the BAM complex and its implications for biogenesis of
323 outer-membrane proteins. *Nat Struct Mol Biol* **23**, 192-196, doi:10.1038/nsmb.3181
324 (2016).

- 325 7 Wu, T. *et al.* Identification of a multicomponent complex required for outer membrane
326 biogenesis in *Escherichia coli*. *Cell* **121**, 235-245 (2005).
- 327 8 Sklar, J. G. *et al.* Lipoprotein SmpA is a component of the YaeT complex that
328 assembles outer membrane proteins in *Escherichia coli*. *Proc Natl Acad Sci U S A* **104**,
329 6400-6405 (2007).
- 330 9 Schiffrin, B., Brockwell, D. J. & Radford, S. E. Outer membrane protein folding from
331 an energy landscape perspective. *BMC Biol* **15**, 123, doi:10.1186/s12915-017-0464-5
332 (2017).
- 333 10 Cho, S. H. *et al.* Detecting Envelope Stress by Monitoring beta-Barrel Assembly. *Cell*
334 **159**, 1652-1664, doi:10.1016/j.cell.2014.11.045 (2014).
- 335 11 Konovalova, A., Perlman, D. H., Cowles, C. E. & Silhavy, T. J. Transmembrane
336 domain of surface-exposed outer membrane lipoprotein RcsF is threaded through the
337 lumen of beta-barrel proteins. *Proc Natl Acad Sci U S A* **111**, E4350-4358,
338 doi:10.1073/pnas.1417138111 (2014).
- 339 12 Tata, M. & Konovalova, A. Improper Coordination of BamA and BamD Results in
340 Bam Complex Jamming by a Lipoprotein Substrate. *MBio* **10**,
341 doi:10.1128/mBio.00660-19 (2019).
- 342 13 Hart, E. M., Gupta, M., Wuhr, M. & Silhavy, T. J. The Synthetic Phenotype of
343 DeltabamB DeltabamE Double Mutants Results from a Lethal Jamming of the Bam
344 Complex by the Lipoprotein RcsF. *MBio* **10**, doi:10.1128/mBio.00662-19 (2019).
- 345 14 Wall, E., Majdalani, N. & Gottesman, S. The Complex Rcs Regulatory Cascade. *Annu*
346 *Rev Microbiol* **72**, 111-139, doi:10.1146/annurev-micro-090817-062640 (2018).
- 347 15 Laloux, G. & Collet, J. F. "Major Tom to ground control: how lipoproteins
348 communicate extra-cytoplasmic stress to the decision center of the cell". *J Bacteriol*,
349 doi:10.1128/JB.00216-17 (2017).

- 350 16 Hussein, N. A., Cho, S. H., Laloux, G., Siam, R. & Collet, J. F. Distinct domains of
351 Escherichia coli IgaA connect envelope stress sensing and down-regulation of the Rcs
352 phosphorelay across subcellular compartments. *PLoS Genet* **14**, e1007398,
353 doi:10.1371/journal.pgen.1007398 (2018).
- 354 17 Kaur, H. *et al.* Identification of conformation-selective nanobodies against the
355 membrane protein insertase BamA by an integrated structural biology approach. *J*
356 *Biomol NMR* **73**, 375-384, doi:10.1007/s10858-019-00250-8 (2019).
- 357 18 Albrecht, R. *et al.* Structure of BamA, an essential factor in outer membrane protein
358 biogenesis. *Acta Crystallogr D Biol Crystallogr* **70**, 1779-1789,
359 doi:10.1107/S1399004714007482 (2014).
- 360 19 Ni, D. *et al.* Structural and functional analysis of the beta-barrel domain of BamA from
361 Escherichia coli. *FASEB J* **28**, 2677-2685, doi:10.1096/fj.13-248450 (2014).
- 362 20 Hartmann, J. B., Zahn, M., Burmann, I. M., Bibow, S. & Hiller, S. Sequence-Specific
363 Solution NMR Assignments of the beta-Barrel Insertase BamA to Monitor Its
364 Conformational Ensemble at the Atomic Level. *J Am Chem Soc* **140**, 11252-11260,
365 doi:10.1021/jacs.8b03220 (2018).
- 366 21 Leverrier, P. *et al.* Crystal structure of the outer membrane protein RcsF, a new
367 substrate for the periplasmic protein-disulfide isomerase DsbC. *J Biol Chem* **286**,
368 16734-16742, doi:10.1074/jbc.M111.224865 (2011).
- 369 22 Rogov, V. V., Rogova, N. Y., Bernhard, F., Lohr, F. & Dotsch, V. A disulfide bridge
370 network within the soluble periplasmic domain determines structure and function of the
371 outer membrane protein RCSF. *J Biol Chem* **286**, 18775-18783,
372 doi:10.1074/jbc.M111.230185 (2011).
- 373 23 Calabrese, A. N. & Radford, S. E. Mass spectrometry-enabled structural biology of
374 membrane proteins. *Methods* **147**, 187-205, doi:10.1016/j.ymeth.2018.02.020 (2018).

- 375 24 Zhang, M. *et al.* A genetically incorporated crosslinker reveals chaperone cooperation
376 in acid resistance. *Nat Chem Biol* **7**, 671-677, doi:10.1038/nchembio.644 (2011).
- 377 25 Gu, Y., Zeng, Y., Wang, Z. & Dong, C. BamA beta16C strand and periplasmic turns
378 are critical for outer membrane protein insertion and assembly. *Biochem J* **474**, 3951-
379 3961, doi:10.1042/BCJ20170636 (2017).
- 380 26 Noinaj, N., Kuszak, A. J., Balusek, C., Gumbart, J. C. & Buchanan, S. K. Lateral
381 opening and exit pore formation are required for BamA function. *Structure* **22**, 1055-
382 1062, doi:10.1016/j.str.2014.05.008 (2014).
- 383 27 Okuda, S. & Tokuda, H. Lipoprotein sorting in bacteria. *Annu Rev Microbiol* **65**, 239-
384 259, doi:10.1146/annurev-micro-090110-102859 (2011).
- 385 28 Storek, K. M. *et al.* Monoclonal antibody targeting the beta-barrel assembly machine
386 of *Escherichia coli* is bactericidal. *Proc Natl Acad Sci U S A* **115**, 3692-3697,
387 doi:10.1073/pnas.1800043115 (2018).
- 388 29 Imai, Y. *et al.* A new antibiotic selectively kills Gram-negative pathogens. *Nature* **576**,
389 459-464, doi:10.1038/s41586-019-1791-1 (2019).
- 390 30 Luther, A. *et al.* Chimeric peptidomimetic antibiotics against Gram-negative bacteria.
391 *Nature* **576**, 452-458, doi:10.1038/s41586-019-1665-6 (2019).
- 392 31 Hart, E. M. *et al.* A small-molecule inhibitor of BamA impervious to efflux and the
393 outer membrane permeability barrier. *Proc Natl Acad Sci U S A* **116**, 21748-21757,
394 doi:10.1073/pnas.1912345116 (2019).
- 395 32 Majdalani, N., Hernandez, D. & Gottesman, S. Regulation and mode of action of the
396 second small RNA activator of RpoS translation, RprA. *Mol Microbiol* **46**, 813-826
397 (2002).

398 33 Baba, T. *et al.* Construction of Escherichia coli K-12 in-frame, single-gene knockout
399 mutants: the Keio collection. *Mol Syst Biol* **2**, 2006 0008, doi:msb4100050 [pii]
400 10.1038/msb4100050 (2006).

401

402

403

404

405

406

407

408

409

410

411

412

413

414

415

416

417

418

419

420

421

422

423 **LEGENDS TO THE FIGURES**

424

425 **Figure 1. RcsF forms a complex with BamAB and BamABCDE.** (a, b) SDS-PAGE (a) and
426 blue native (b) analysis of purified BAM, BAM-RcsF and BamAB-RcsF complexes obtained
427 via BamA-affinity chromatography. The bands analyzed in (c) are labelled 1 to 8. (c) SDS-
428 PAGE analysis of the complexes shown in panel b (bands 1 to 8). The BAM complex expressed
429 from pRRA1 is a mixture of BamABCDE and BamABDE. n= 4 biologically independent
430 experiments.

431

432 **Figure 2. Structure of the BamA-RcsF complex.** (a) Ribbon diagram of the BamA-RcsF
433 complex in side view. BamA, gold; RcsF, blue. (b, c) Front (b) and extracellular (c) views of
434 BamA-RcsF, with RcsF shown as a solvent-accessible surface. POTRA domains 1 and 2 have
435 been omitted for clarity. BamA ^εL6, green; ^ϕL4, magenta. Putative RcsF-interacting residues
436 in contact zones Z1 and Z2 of the BamA β-barrel are colored cyan and magenta, respectively,
437 and shown as sticks. Strands β1 and β16, which form the proposed “lateral gate” of the BamA
438 β-barrel ¹, are yellow. (d) Periplasmic view of the BamA-RcsF complex, with the BamA β-
439 barrel shown as a solvent-accessible surface and RcsF as a ribbon. Colors are as in panels b
440 and c. POTRA domains were omitted for clarity.

441

442 **Figure 3. Conformational characteristics of the BamA-RcsF complex.** (a, c) Tilted top view
443 and slabbed side view of the overlay of the BamA-RcsF complex and BamA in the outward-
444 open conformation (grey, taken from BamACDE complex PDB:5EKQ ⁴). The BamA β-barrel
445 undergoes a ~45° outward rotation at strands β1-β6, and a 20 Å inward displacement of
446 POTRA5 compared to the structure of BamA-RcsF presented here. (b) Slabbed side view of
447 the overlay of BamA-RcsF and BamA in the inward-open conformation (grey, taken from

448 BamABCDE complex PDB:5D0O⁵). In the structure of BamA-RcsF presented here, POTRA5
449 makes a 26° outward rotation relative to R421, where it connects to the BamA β-barrel. **(a-c)**
450 Color scheme for BamA-RcsF is as in Fig. 2b. RcsF is shown as a solvent-accessible surface
451 (a) or a ribbon (b, c). Panels (b, c) show side views, slabbed down to view the interior of the
452 complex. For 5EKQ and 5D0O, the BAM accessory proteins BamB, C, D, and E were omitted
453 for clarity, as were POTRA domains 1-4 in all shown BamA structures.

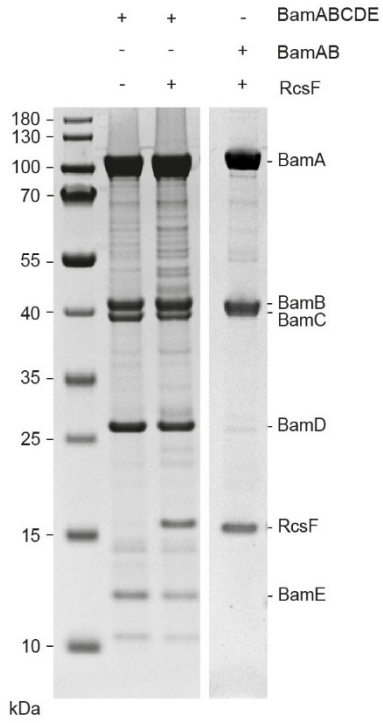
454

455 **Figure 4. BamA-RcsF is a proxy for the inward-open conformation of BamA. (a)** *In vivo*
456 chemical crosslinking of RcsF with BamA and OmpA. The BamA-RcsF complex accumulates
457 when either BamA alone or BamAB together are moderately over-expressed from a plasmid
458 in cells also expressing BAM at physiological levels from the chromosome. The copies of
459 BamA and BamAB in excess are not functional (BamCDE is required for BAM activity) and
460 do not funnel RcsF to its OMP partners. As a result, RcsF accumulates on BamA and OmpA-
461 RcsF does not form. Over-expression of BamCDE (also from a plasmid) in these cells restores
462 the stoichiometry between the BAM components: BamA-RcsF does not accumulate and the
463 formation of OmpA-RcsF is restored. As shown previously¹⁰, levels of OmpA-RcsF are
464 inversely correlated with BamA-RcsF. Overexpression of the BamCDE sub-complex alone
465 does not impact the activity of the BAM complex expressed from the chromosome: wild-type
466 BamA-RcsF and OmpA-RcsF levels are observed. Wild-type BamA-RcsF and OmpA-RcsF
467 levels are also detected when BamA and BamCDE are overexpressed together, as expected
468 given that BamB is not essential. RcsF also forms a complex with the abundant lipoprotein Lpp
469 (Lpp-RcsF), as in¹⁰. Protein expression levels of OmpA were analyzed by immunoblot in the
470 non-crosslinked samples, showing no differences. The additional bands that are detected in the
471 lanes where BamA-RcsF is not observed likely correspond to poorly abundant complexes
472 between RcsF and unknown proteins. n= 3 biologically independent experiments. **(b)** Protein

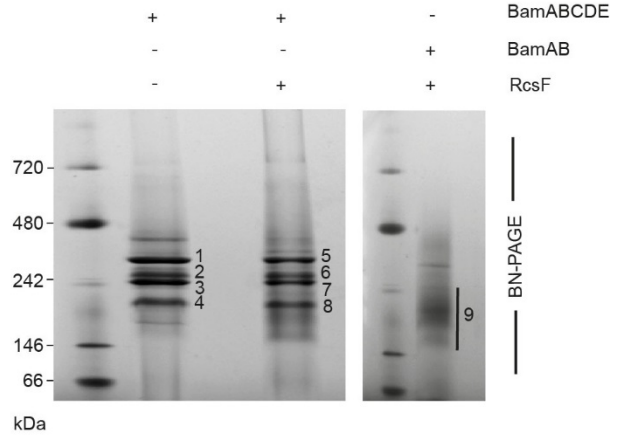
473 expression levels of BamB, BamC, BamD, BamE and RcsF from no-crosslinked samples
474 overexpressing BamA (pBamA), BamAB (pBamA-B) and BamCDE (pSC263) were analyzed
475 by western blot. EF-Tu expression levels were analyzed as loading control. n= 3 biologically
476 independent experiments. (c) Model proposing that BamA conformational cycling is triggered
477 by incoming OMP substrates on the BAM holocomplex. A BamA inward-to-outward open
478 transition could result in an upward displacement of RcsF via a push-and-pull mechanism,
479 resulting in an OMP-RcsF complex. The push-and-pull mechanism involves BamA POTRA5
480 (P5) and Z1. The topology of the OMP-RcsF complex remains to be established. For clarity,
481 POTRA1-4 and the BAM lipoproteins have been omitted.

Figure 1

a



b



c

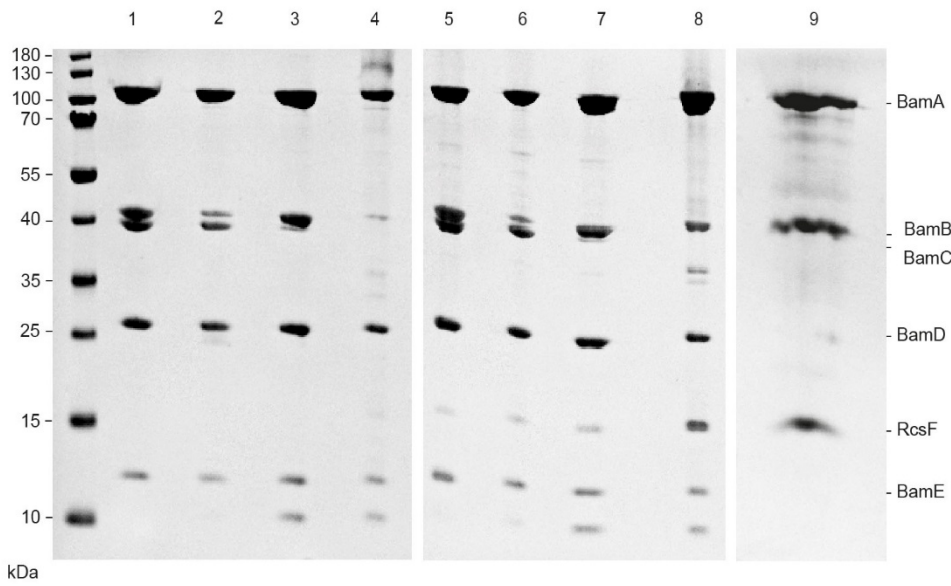


Figure 2

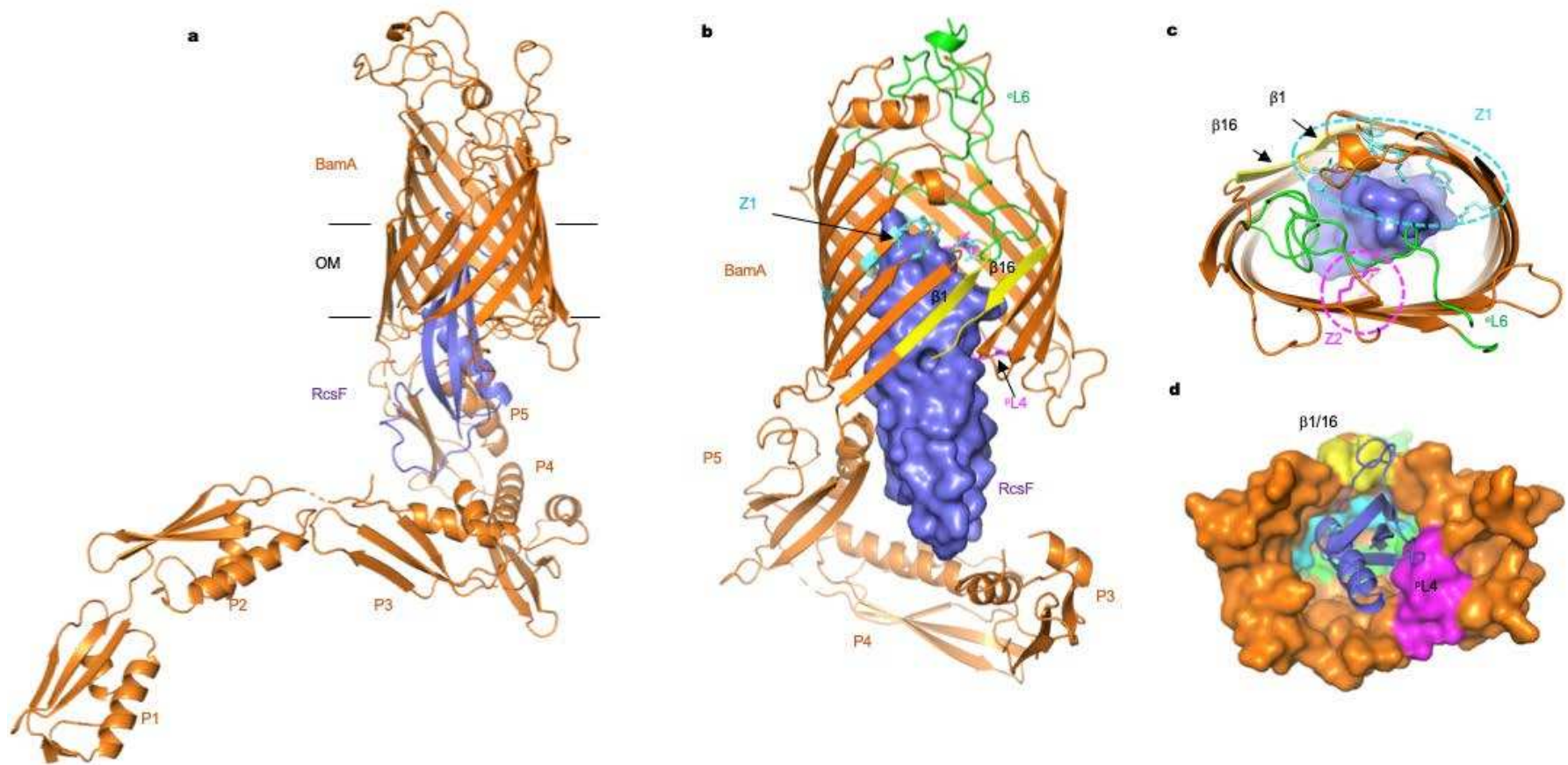


Figure 3

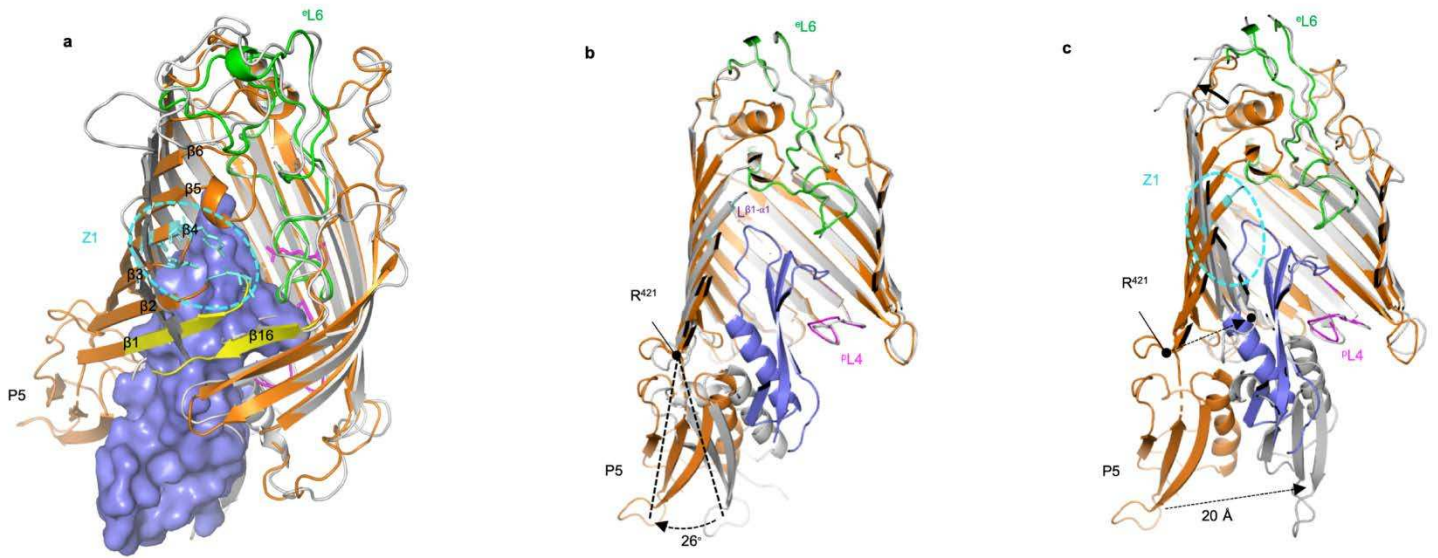
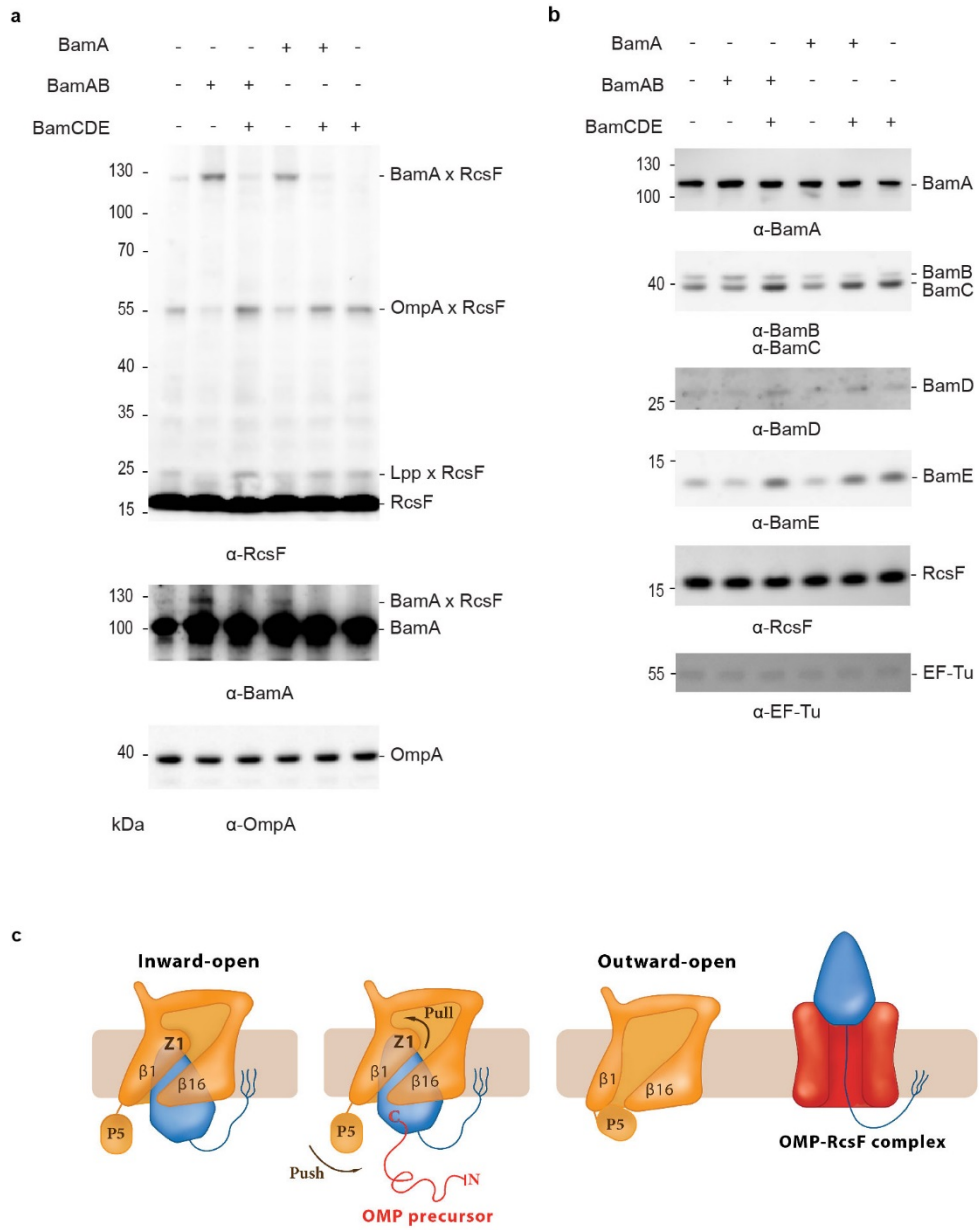


Figure 4



484 **METHODS**

485

486 **Bacterial strains, plasmids, and primers**

487 Bacterial strains and plasmids used in this study are listed in Supplementary Tables 3 and
488 4, respectively. The parental *E. coli* strain DH300 is a MG1655 derivative deleted for the
489 *lac* region and carrying a chromosomal *rprA_P::lacZ* fusion at the λ phage attachment site
490 to monitor Rcs activation³². To delete *bamA* on the chromosome, a kanamycin resistance
491 (*kan*) cassette³³ with the flanking regions of *bamA* was PCR amplified from the genomic
492 DNA of a Δ *rcsF::kan* strain (PL339) using primers “bamA Km del F” and “bamA Km
493 del R”. Then we performed λ -Red recombineering³⁴ with plasmid pSIM5-tet³⁵ on the
494 strain containing pSC270 as a *bamA*-complementing plasmid in DH300. Deletion of
495 *bamA* was verified by PCR. After preparing P1 lysate from this strain, *bamA* deletion (by
496 transferring the *kan* cassette) was performed via P1 phage transduction of the appropriate
497 strains.

498

499 We performed site-directed mutagenesis to generate *bamA* variants on plasmids. For
500 single-codon changes, primer sequences are available upon request; otherwise see
501 Supplementary Table 5. By using pJH114 as a template and performing site-directed
502 mutagenesis (SDM), we introduced a six-histidine tag at the N-terminus of BamA. The
503 C-terminal His-tag of BamE was also removed via SDM, generating pRRA1. The primer
504 pairs were “SDM-HisBamA F” with “SDM-HisBamA R” and “bamE delHis F” with
505 “bamE delHis R”. To add *bamB* next to *bamA* in pBamA, both *bamA* and *bamB* were
506 PCR amplified as a single DNA fragment from pJH114³⁶ using primers “pTrc-for” and
507 “bamB (NotI) R”. The PCR product and pBamA were digested with NcoI and NotI and
508 then ligated, yielding pBamA-B. pBamA^{hinge} plasmid was generated by SDM using

509 primers “BamA hinge F” and “BamA hinge R” and pBamA as template. To clone *bamC*,
510 *bamD*, and *bamE* as an operon into a low-copy plasmid (pAM238), PCR was performed
511 on pRRA1 as a template using primers “bamC kpnI F” and “pTrc-rev2”. The PCR product
512 and pAM238 were digested with KpnI and XbaI and ligated, generating pSC263. We
513 cloned *bamA* without the six-histidine tag into the low-copy plasmid pSC23¹⁰, yielding
514 pSC270. *bamA* was PCR amplified from *E. coli* genomic DNA using primers “BamA
515 (PciI)F” and “BamA (XbaI)R” and ligated with pSC231 predigested with NcoI and XbaI.
516 To generate the *bamA* variants locked in the closed and open conformations, SDM was
517 performed on pBamA-B. First, the two cysteines in the ^εL6 loop of BamA were mutated
518 to serines, generating pBamA_{L6}-B. This plasmid was used as template for SDM to
519 generate pBamA^{G393C/G584C}-B and pBamA^{G433C/N805C}-B. To generate *bamA* variants with
520 amber codons (TAG) to insert 3-(3-methyl-3H-diazirine-3-yl)-propaminocarbonyl-N ϵ -L-
521 lysine (DiZPK; Artis Chemistry, Shanghai) at selected positions, we performed SDM on
522 pBamA-B and pSC270; primer sequences are available upon request.

523

524 **Expression and purification of the BamAB-RcsF complex**

525 *E. coli* PL358 cells harboring pJH118 expressing N-terminal six-histidine-tagged BamA
526 and BamB³⁶ and pSC216 expressing RcsF¹⁰ were cultured to overexpress BamA, BamB,
527 and RcsF. Cells were grown in Terrific Broth Auto Inducing Medium (Formedium)
528 supplemented with 0.2% (w/v) L-arabinose at 37 °C (to induce RcsF), ampicillin (200
529 μ g/mL), and chloramphenicol (25 μ g/mL). Cells (1 L) were pelleted when they reached
530 OD₆₀₀ ~ 4, re-suspended in cold phosphate-buffered saline (25 mL) containing a protease-
531 inhibitor cocktail (Complete, Roche), and lysed by two passages through a French
532 pressure cell at 1,500 psi. The cell lysate was centrifuged for 40 min at 40,000 \times g and 4
533 °C. After centrifugation, inner-membrane proteins were solubilized using 0.5% (w/v) N-

534 lauryl sarcosine (Sigma) in a buffer containing 20 mM Tris-HCl [pH 7.5] and 150 mM
535 NaCl for 1.5 h at 4 °C on a roller. The suspension was centrifuged for 40 min at 40,000
536 x g and 4 °C, after which the inner membrane fraction was in the supernatant while the
537 outer membrane fraction remained in the pellet. Outer-membrane proteins were
538 solubilized using 1% (w/v) *n*-dodecyl- β -d-maltopyranoside (DDM; Anatrace) in a buffer
539 containing 20 mM Tris-HCl [pH 7.5], 300 mM NaCl, and 20 mM imidazole overnight at
540 4 °C on a roller. After centrifugation (40,000 x g, 4 °C, 40 min), the supernatant was
541 mixed with Ni-NTA agarose beads (2 mL; IBA Lifescience) equilibrated with 20 mM
542 Tris-HCl [pH 7.5], 300 mM NaCl, 20 mM imidazole, and 1% (w/v) DDM. After washing
543 the resin with 10 column volumes of buffer (20 mM Tris-HCl [pH 7.5], 150 mM NaCl,
544 20 mM imidazole, 0.6% (w/v) tetraethylene glycol monoethyl ether (C8E4; Anatrace),
545 and 0.01% (w/v) DDM), proteins were eluted with 5 column volumes of the same buffer
546 supplemented with 200 mM imidazole. The eluted complex was then concentrated to 1
547 mL using a Vivaspin 4 Turbo concentrator (Cut-off 5 kDa; Sartorius). A final purification
548 step was performed using size-exclusion chromatography by loading the proteins on a
549 HiLoad 10/300 Superdex 200 column (GE Healthcare) using 20 mM Tris-HCl [pH 7.5],
550 150 mM NaCl, 0.6% (w/v) C8E4, and 0.01% (w/v) DDM. Peak fractions were pooled
551 and concentrated to ~30 mg/mL for crystallization.

552

553 For co-crystallization with NaI, NaI replaced NaCl in the gel-filtration buffer. Peak
554 fractions were pooled and concentrated to ~30 mg/mL using a Vivaspin 4 Turbo
555 concentrator (Sartorius).

556

557 The Blue native electrophoresis analysis of the concentrated complex was carried out on
558 a 3-12% Bis-Tris gel (Life Technologies) following the manufacturer's instructions. The

559 protein complex bands separated in the native electrophoresis were identified via SDS-
560 PAGE. Briefly, bands of interest were excised, boiled in SDS-PAGE sample buffer, and
561 applied to the top of a polyacrylamide gel.

562

563 **Expression and purification of BAM (BamABCDE) in complex with RcsF**

564 *E. coli* BL21 (DE3) was transformed with pRRA1 expressing all five BAM proteins (N-
565 terminal six-histidine-tagged BamA, BamB, BamC, BamD, and BamE) and pSC216
566 expressing RcsF for BAM and RcsF overexpression. In control cells, only pRRA1 was
567 transformed. Protein expression and purification were performed as described above
568 except that the detergent was exchanged to 0.1% (w/v) DDM during Ni-NTA affinity
569 chromatography and size-exclusion chromatography. Eluted complexes were identified
570 via SDS-PAGE and concentrated to 4 mg/mL. Blue native electrophoresis of the
571 concentrated complexes was carried out as described above.

572

573 **Crystallization, data collection and structure determination**

574 Crystallization assays were carried out using the hanging drop vapor diffusion method in
575 48-well plates (Molecular Dimensions) at 20°C. The protein solution was mixed in a 2:1
576 ratio with the crystallization solution from the reservoir. The best native crystals were
577 grown after 4 to 5 days in C10 and G10 conditions from Morpheus crystallization screen
578 (Molecular dimensions; C10: 0.03 M sodium nitrate, 0.03 M sodium phosphate dibasic,
579 0.03 M ammonium sulfate, 0.10 M Tris-base [pH 8.5]; BICINE, 20 % (v/v) ethylene
580 glycol; 10 % w/v PEG 8000; G10: 0.02 M sodium formate; 0.02 M ammonium acetate;
581 0.02 M sodium citrate tribasic dihydrate; 0.02M potassium sodium tartrate tetrahydrate;
582 0.02 M sodium oxamate; 0.10 M Tris-base [pH 8.5]; BICINE; 20% (v/v) ethylene glycol;
583 10 % (w/v) PEG 8000).

584

585 The crystals were harvested in a nylon loop, flash-cooled and stored in liquid nitrogen for
586 data collection. Crystals were screened on beamlines Proxima-1 and Proxima-2 at
587 Synchrotron Soleil (Gif-sur-Yvettes, France) as well as beamlines I03 and I04-1 at
588 Diamond Light Source (Didcot, UK). Data for structure determination were collected on
589 the Proxima-2 beam-line at Synchrotron Soleil at a wavelength of 1.77 Å. Data were
590 indexed and integrated using XDS³⁷, scaled using XSCALE³⁷ and anisotropically
591 corrected using STARANISO, applying a high resolution cutoff of $I/\sigma I = 1.2$ ³⁸. The
592 crystals belong to space group C2, with the unit cell dimensions $a=158.84$, $b=142.5300$,
593 $c=116.4200$ Å³ and $\beta=102.61^\circ$. The structure was determined by molecular replacement
594 using Phaser³⁹, with the globular domain of RcsF (residues 51-130, PDB:2Y1B) and the
595 inward open BamA β -barrel (residues 422-809, PDB: 5D0O) and BamA POTRA domain
596 4 (residues 265-344; PDB: 5D0O) as search models. Molecular replacement searches
597 identified two copies each of the BamA β -barrel, RcsF and POTRA domain 4. Following
598 10 cycles of rigid body refinement POTRA domains 1, 2, 3 and 5 of the first BamA-RcsF
599 copy in the asymmetric unit (Extended Data Figure 2) could be manually placed in the
600 2FoFc and FoFc difference density and were subjected to an additional 10 rounds of rigid
601 body refinement. The model was refined to 3.8 Å resolution using BUSTER⁴⁰ and
602 intermittent manual inspection and correction of the model in Coot⁴¹. BUSTER was run
603 using Local Structure Similarity Restraints (LSSR) over the two copies in the asymmetric
604 unit, as well as target-based similarity restraints using the inward open BamA structure
605 as reported in PDB:5D0O. The final model shows R and freeR factors of 28.3% and
606 31.4%, respectively, containing 1388 amino acids, of which 19 are indicated as
607 Ramachandran outliers (1.4%). We note that side chain positioning is frequently
608 ambiguous at 3.8 Å resolution and should therefore not be over-interpreted by users of

609 the deposited model. Side chains for which no unambiguous electron density was
610 observed were not pruned for ease of model interpretation. Such side chains were
611 included in refinement and manually modelled in their most likely rotamer using Coot.
612 Data collection and refinement statistics are found in Supplementary Table 1.

613

614 **Site-specific photo-crosslinking**

615 We used a site-specific photo-crosslinking method described previously ¹⁰ with some
616 modifications. To incorporate DiZPK into BamA, we used the pSup-Mb-DIZPK-RS
617 plasmid encoding an evolved *Methanosarcina barkeri* pyrrolysyl-tRNA synthetase and
618 an optimized tRNA_{CUA}^{Pyl} suppressor ²⁴. DH300 cells were co-transformed with pSup-Mb-
619 DIZPK-RS and one of the plasmids containing an amber codon in BamA in pSC270.
620 Cells were grown in 3-(N-morpholino) propanesulfonic acid (MOPS) minimal medium
621 supplemented with 0.2% glucose, 0.2% (w/v) arabinose, 200 μM IPTG, 0.001% (w/v)
622 casamino acids, and 0.8 mM DiZPK. When cells reached OD₆₀₀ = 1, 500-μL samples
623 were irradiated with ultraviolet light at 365 nm or left unirradiated for 10 min. Cells were
624 precipitated with trichloroacetic acid, washed with ethanol, and proteins were solubilized
625 in 100 μL SDS-PAGE sample buffer (50 mM Tris-HCl [pH 7.5], 1% (w/v) SDS, 10%
626 (v/v) glycerol, 0.002% (w/v) bromophenol blue) before SDS-PAGE and immunoblotting
627 using anti-RcsF and anti-BamA antibodies.

628

629 ***In vivo* BS3 crosslinking**

630 Cells were harvested around mid-log phase (OD₆₀₀ = ~ 0.5). *In vivo* crosslinking was
631 performed as described previously ¹⁰, except that bis(sulfosuccinimidyl)suberate
632 (CovaChem) was used instead of 3,3'-dithiobis(sulfosuccinimidyl propionate).

633

634 **Chemical crosslinking-mass spectrometry**

635 We first performed buffer exchange of the purified BamAB-RcsF complex using a PD-
636 10 desalting column (GE Healthcare Life Sciences). The complex was eluted with 20 mM
637 HEPES [pH 7.5], 150 mM NaCl, and 0.1% (w/v) DDM. A 30-fold molar excess of the
638 crosslinker disuccinimidyl dibutyric urea (50 mM stock solution in dimethyl sulfoxide,
639 Thermo Scientific) was added to the protein solution and incubated at 37 °C for 1 h. The
640 reaction was quenched by adding Tris-HCl to a final concentration of 20 mM. Crosslinked
641 proteins were precipitated with ethanol and trypsinized, and crosslinked peptides were
642 enriched through cation exchange as described previously⁴². Briefly, crosslinked proteins
643 (50 µL) were precipitated by adding ice-cold ethanol (150 µL) and 3 M sodium acetate
644 [pH 5.3] (5 µL) prior to incubation at -20 °C for 16 h. The sample was centrifuged
645 (16,200 x g, 4 °C, 30 min), the supernatant was removed, and the pellet was washed by
646 adding 80% (v/v) ice-cold ethanol (200 µL) and vortexing for 30 s. The sample was
647 centrifuged again, the supernatant was removed, and the pellet was dried in a vacuum
648 centrifuge. The pellet was dissolved in 1% (w/v) RapiGest (Waters) (10 µL) and trypsin
649 (Sequencing grade, Promega) solution was added (90 µL, 1:50 trypsin:protein mass ratio)
650 before incubating overnight at 37 °C. Trifluoroacetic acid was added (final concentration
651 0.5% (v/v)) and the sample was incubated at 37 °C for 1 h to precipitate the Rapigest. The
652 mixture was centrifuged (16,200 x g, 4 °C, 30 min), the supernatant was concentrated
653 using a vacuum centrifuge, and the pellet was dissolved in 20% (v/v) acetonitrile/0.4%
654 (v/v) formic acid (20 µL). Strong cation exchange enrichment was carried out using
655 OMIX 10 µL strong cation exchange pipette tips (Agilent) as previously described⁴².
656
657 Fractionated peptides (5 µL) were injected onto a reverse-phase Acquity M-Class C18,
658 75 µm x 150 mm column (Waters) and separated via gradient elution of 1-50% (v/v)

659 solvent B (0.1 % (v/v) formic acid in acetonitrile) in solvent A (0.1 % (v/v) formic acid
660 in water) over 60 min at 300 nL/min. The eluate was infused into a Xevo G2-XS (Waters)
661 mass spectrometer operating in positive ion mode. Mass calibration was performed by
662 infusion of aqueous NaI (2 µg/µL). [Glu1]-Fibrinopeptide B was used for the lock mass
663 spray, with a 0.5 s lock spray scan taken every 30 s. The lock mass correction factor was
664 determined by averaging 10 scans. Data acquisition was performed in DDA mode with a
665 1 s mass-spectrometry scan over m/z 350-2000. Instrument parameters were optimized
666 for the detection of crosslinked peptides, as described previously ⁴³. Data processing and
667 crosslink identification were performed using MeroX ⁴⁴.

668

669 **Expression of BamA mutants and co-purification with RcsF**

670 pBamA and pBamA-B each provide chromosomal-level expression of BamA ¹⁰.
671 Therefore, we introduced mutations of *bamA* in these plasmids to test the physiological
672 effects of BamA mutants; plasmids were expressed in the presence or absence of *bamA*
673 on the chromosome. Cells (2 mL) were harvested at OD₆₀₀ ~ 0.5 to purify BamA, except
674 during the following experiment. The cysteine mutants of BamA, when oxidized to form
675 a disulfide bond, allow BamA to form an “open” or “closed” lateral gate. Therefore, the
676 efficiency of disulfide-bond formation in these mutants is very important. To enhance the
677 oxidation of cysteines to form disulfide bonds, we added 3 mM tetrathionate as an oxidant
678 ⁴⁵ at OD₆₀₀ ~ 0.5 and harvested cells (1 mL) at OD₆₀₀ ~ 1.0.

679

680 Since there was a six-histidine tag at the N-terminus of BamA, we used Dynabeads™
681 His-Tag (Invitrogen) for Ni-affinity purification. After resuspending cells in 350 µL of
682 25 mM Tris-HCl [pH 7.4], 290 mM NaCl, 1 mM imidazole, and 0.05% (w/v) DDM
683 (buffer A), cells were lysed via mild sonication on ice. Membrane vesicles were further

684 solubilized by increasing the DDM concentration to 1% (w/v). After removing debris via
685 centrifugation at $9,300 \times g$ for 10 min, 5 μL of Dynabeads™ His-Tag (pre-washed with
686 buffer A and resuspended in the same volume) were added to 250 μL of the supernatant,
687 which was incubated for 20 min at 4 °C. The rest of the supernatant was used as the input
688 fraction. The magnetic beads were pulled by a magnet and the supernatant was taken for
689 the flow-through fraction. After washing the beads three times with 750 μL buffer E using
690 the magnet, bound proteins were eluted with 83 μL (three times enrichment compared to
691 the other fractions) of buffer A with 300 mM imidazole. Forty microliters of the input,
692 flow-through, and elution fractions were mixed with SDS-PAGE sample buffer. After
693 denaturation of the three fractions, SDS-PAGE was performed, followed by
694 immunoblotting using rabbit-raised anti-BamA, anti-RcsF¹⁰, anti-BamB, anti-BamC,
695 anti-BamD, and anti-BamE.

696

697 To determine the redox states of the cysteine-introduced gate mutants of BamA, we added
698 3 mM N-ethylmaleimide in SDS-PAGE sample buffer to alkylate cysteines to prevent
699 thiol-disulfide exchange. The sample was divided into two aliquots and 10 mM of tris(2-
700 carboxyethyl) phosphine was added to one of them to obtain the reduced state of BamA
701 as a control. Nu-PAGE (4-12% gradient; Novex) was used to separate the oxidized and
702 reduced bands of BamA.

703

704 **Spotting assay for growth.** Cells were grown in M9 minimal glucose medium at 30°C
705 until they reached $\text{OD}_{600} = 1$. Tenfold serial dilutions were made in M9 minimal glucose,
706 plated onto M9 minimal glucose or LB agar, and incubated at 30°C or 37°C. Plates were
707 supplemented with ampicillin (200 $\mu\text{g}/\text{ml}$).

708

709 **Biolayer interferometry**

710 Untagged BamA was first biotinylated using the EZ-Link NHS-PEG4-biotin kit (Perbio
711 Science). The reaction was stopped by adding Tris [pH 8] to the final concentration of 20
712 mM. Excess NHS-PEG4-biotin was removed by passing the sample through a Zeba Spin
713 Desalting column (Perbio Science). Biolayer interferometry was performed in black 96-
714 well plates (Greiner) at 25 °C using OctetRed96 (ForteBio). Streptavidin and Ni-NTA
715 biosensor tips (ForteBio) were hydrated with 0.2 mL working buffer (20 mM Tris [pH
716 8], 150 mM NaCl, 0.03 % (w/v) DDM) and then loaded with biotinylated BamA or 6xHis-
717 tagged RcsF, respectively.

718

719 In the forward experiment, purified 6xHis-tagged RcsF (5 µg/mL) was immobilized on
720 Ni-NTA sensors until the signal reached 0.5-0.6 nm. Association and dissociation of
721 BamA to RcsF-coated tips were monitored for 1200 s and 300 s, respectively, by dipping
722 tips into BamA-containing buffer (serial two-fold dilution from 4000 nM to 62.5 nM),
723 and subsequently in buffer only. In the reverse experiment, biotinylated BamA was
724 immobilized on streptavidin sensor tips to a signal of 2.0 nm. The association and
725 dissociation of RcsF (serial 3-fold dilution from 3000 nM to 12.34 nM) to BamA-coated
726 tips were monitored for 4800 s and 700 s, respectively. Dissociation constants were
727 determined using Graphpad Prism by linear regression of the steady-state binding
728 responses in the saturation binding experiment (Extended Data Fig. 4c, d).

729

730 For binding of the BamA^{G393C/G584C} mutant (Extended Data Fig. 5c), 6xHis-tagged RcsF
731 was immobilized on Ni-NTA sensors. To follow BamA association and dissociation,
732 RcsF-coated tips were dipped into 0.2 mL of 200 nM BamA solution, with or without 2
733 mM dithiothreitol, for 1200 s, followed by 1200 s in buffer only.

734

735 **Antibodies and immunoblotting**

736 Rabbit anti-RcsF antibody was previously generated and used by us ¹⁰. We newly raised
737 the antibodies against BamA, BamB, BamC, BamD, and BamE in rabbits as follows.
738 Except BamA, the DNA sequences encoding the proteins without the signal sequence
739 were cloned into pET28a (Novagen) using the NcoI and XhoI restriction sites, which
740 allows the expressed proteins to be his-tagged at the C-terminus. For BamA, DNA
741 encoding the POTRA domains (1-4) of BamA with a C-terminal strep-tag (but without
742 the signal sequence) was cloned in pET21a (Novagen). All the proteins above were
743 overexpressed in BL21(DE3) and purified using standard methods for Ni-NTA affinity
744 purification or streptavidin purification (POTRA 1-4). Small aliquots of the purified
745 proteins were sent to the CER group (Marloie, Belgium) to raise antibodies in rabbits.
746 Goat Anti-Rabbit IgG alkaline phosphatase conjugated (Sigma) was used as a secondary
747 antibody at a 1:20,000 dilution.

748

749 Antibody specificity was confirmed by comparing the immunoblot of the wild-type strain
750 with that of a mutant using each corresponding antibody. The dilutions of the antibodies
751 for immunoblotting were 1:10,000 (BamA), 1:20,000 (BamB), 1:40,000 (BamC),
752 1:10,000 (BamD), and 1:20,000 (BamE). The specificity of the antibodies was verified;
753 data are available upon request.

754

755 To simplify the detection of Bam components and RcsF after purification of BamA, we
756 used two mixtures of antibodies (anti-BamA plus anti-RcsF; anti-BamB, anti-BamC, anti-
757 BamD, plus anti-BamE). Detection specificity was verified using similar mutants as
758 above but harboring pBamA. Data are available upon request.

759

760 The antibody recognizing the transmembrane domain of OmpA is a gift from the
761 Bernstein laboratory ⁴⁶. The rabbit polyclonal OmpC antibody was purchased from
762 EPIGENTEK. The anti-*E. coli* EF-Tu antibody (mAb 900) was purchased from
763 HycultBiotech. The Goat anti-mouse IgG conjugated with the Cy3 fluorescent dye was
764 used as a secondary antibody for EF-Tu (Amersham).

765

766 **β -galactosidase assay**

767 Rcs induction was monitored by measuring β -galactosidase activity as described ⁴⁷.
768 Briefly, cells harboring *PrprA-lacZ* at the *attB* phage lambda site on the chromosome
769 were diluted 1:100 from overnight cultures in Luria broth (LB), then incubated at 37°C.
770 Cells were harvested at OD₆₀₀ = 0.6-1. Twenty microliters of cells were harvested and
771 incubated with 80 μ l of permeabilization solution (60 mM Na₂HPO₄·2H₂O, 40 mM
772 NaH₂PO₄·H₂O, 10 mM KCl, 1 mM MgSO₄·7H₂O, 50 mM β -mercaptoethanol) for 30–45
773 min at room temperature. Then, 600 μ l of substrate (1 mg/ml O-nitrophenyl- β -d-
774 galactoside, 50 mM β -mercaptoethanol) were added. The mixture was further incubated
775 at 30°C for 20-90 min. Seven hundred microliters of 1 M Na₂CO₃ were added to stop the
776 reaction, and the optical density was measured at 420 nm. The standardized amount of β -
777 galactosidase activity was reported in Miller units. The ratio of *PrprA-lacZ* induction was
778 calculated relative to the basal level in a WT strain. Bar graphs with corresponding
779 statistical analysis were prepared using Prism 7 (GraphPad Software, Inc.).

780

781 **Statistical methods**

782 The significance of differences among bacterial strains was assessed using GraphPad
783 Prism 8 according to analysis of variance (two ways ANOVA), followed by the

784 application of Tukey's multiple-comparison test. Normality was assessed using the
785 Shapiro-Wilk test.

786

787 **Molecular modeling: protein insertion in the lipid bilayer**

788 The initial simulation system was prepared starting from the BamA-RcsF complex
789 determined in this work (PDB code 6T1W) with the POTRA1-4 domains removed.

790 Missing residues and C-terminal residues of BamA and RcsF were completed with
791 MODELLER v9.22⁴⁸ to generate a protein complex containing residues 347-810 for

792 BamA and 51-134 for RcsF. This complex was preorientated with respect to the
793 membrane normal (z axis) using the structure 5AYW⁶ from the OPM database

794 (<https://opm.phar.umich.edu>)⁴⁹ as template, then embedded in an asymmetric bilayer to
795 mimic the *E. coli* outer membrane using CHARMM-GUI (<http://www.charmm-gui.org>)

796⁵⁰ and following the protocols described for OmpLA⁵¹ and BamA⁵²). The inner leaflet
797 was a mixture of 100 lipids: 75 1-palmitoyl(16:0)-2-palmitoleoyl(16:1 *cis*-9)-

798 phosphatidylethanolamine (PPPE), 20 1-palmitoyl(16:0)-2-vacenoyleoyl(18:1 *cis*-11)-
799 phosphatidylglycerol (PVPG), and 5 1,10-palmitoyl-2,20-vacenoyleoyl cardiolipin with a net

800 charge of $-2e$ (PVCL2), corresponding to a ratio of 15:4:1. The outer leaflet was
801 composed of 36 LPS (including the lipid A, R1 core and O-antigen polysaccharide

802 fragments). The equilibration was performed according to the standard protocol from
803 CHARMM-GUI Membrane Builder, with restraints that were gradually reduced in 6

804 steps (2.125 ns overall), using CHARMM version 44b1⁵³. A similar protocol was used
805 to build a second system, containing the outward-open conformation of BamA (PDB code

806 5D0Q)⁵ with the POTRA1-4 domains removed and the RcsF from 6T1W shifted upwards
807 on the z axis by 30 Å.

808

809 **Dynamic importance sampling simulations**

810 Dynamic importance sampling (DIMS) uses a biasing with correction approach to
811 improve the sampling efficiency of rare events. The *soft ratcheting* algorithm generates
812 transitions between states using a stochastic approach⁵⁴. It should be noted that at any
813 point of the DIMS simulation the intermediate system is realistic (no force is applied and
814 the potential function is not modified) and the simulated pathway is always possible,
815 although it may not be in all cases the lowest energy one. In this work, we carried out
816 DIMS Langevin dynamics (LD) simulations using CHARMM version 44b1 (collision
817 frequency of 25.0) starting from the first system and with the second system as target.
818 The “soft-ratcheting” implemented in DIMS accepts all steps proceeding towards the
819 desired final state and a fraction of steps away from the target. This fraction is defined by
820 DIMS-Cartesian for which we used the recommended value of 10^{-6} ⁵⁵. Two replicas were
821 simulated, providing similar results, and only the results from the first replica are
822 presented here.

823

824 **Image and video rendering**

825 The pictures representing molecular data were generated using PyMOL version 2.2.0
826 (Schrödinger LLC, <https://pymol.org>). The video was generated from the DIMS
827 simulation (replica 1) using VMD⁵⁶.

828 **LEGENDS TO EXTENDED DATA FIGURES**

829

830 **Extended Data Figure 1. RcsF can be co-purified with the BAM complex. (a,b,c)** Gel
831 filtration profiles of the affinity-purified BamAB-RcsF, BAM-RcsF and BAM
832 complexes. The size exclusion chromatography was performed using a HiLoad 10/300
833 Superdex 200pg. The input and peak fractions were collected and the samples were
834 analyzed by blue native electrophoresis with Coomassie staining. The migration pattern
835 of BamABCDE-RcsF (b) was modified compared to BamABCDE (c) upon size exclusion
836 chromatography (band 8 increases), reflecting the higher instability of the BamABCDE-
837 RcsF complex. n= 4 biologically independent experiments.

838

839 **Extended Data Figure 2. Crystal structure of the BamA-RcsF complex. (a, b)** Final
840 2Fo-Fc electron map of the BamA-RcsF complex, shown with a map contour level of
841 $0.08 \text{ e}/\text{\AA}^3$ (root mean square deviation 1.02 \AA). The asymmetric unit of the crystals holds
842 two BamA-RcsF copies, one revealing interpretable electron density for the full BamA
843 sequence (a), and a second revealing unambiguous density for POTRA domain 4 only
844 (b). In the second copy (b), the electron density corresponding to POTRA domains 1, 2,
845 3, and 5 is too weak to allow unambiguous rigid body placement of the domains. All
846 descriptions and images in the main text are based on the first copy (a). (c) Overlay of
847 two BamA-RcsF complexes in the asymmetric unit. The first complex depicts BamA in
848 gold and RcsF in blue, while these molecules are yellow and light blue, respectively, in
849 the second complex. In both copies, RcsF makes an average displacement of 4 \AA relative
850 to the BamA β -barrel. (d) Crystal packing of the BamA-RcsF complex viewed along the
851 a- (left) and c-axis (right). For the first copy of the BamA-RcsF complex in the
852 asymmetric unit (orange-slate) the conformation of the POTRA domains is stabilized by

853 the packing along the b-axis, whilst for the second copy (cyan-slate) only POTRA domain
854 4 is involved in crystal contacts. In the latter, POTRA 5, 3, 2 and 1 are not in contact with
855 neighboring molecules and show weak electron density only due to the lack of
856 conformational stabilization.

857

858 **Extended Data Figure 3. Structural dynamics of the BamA POTRA domains. (a, b)**

859 Superimposition of BamA-RcsF (gold and blue, respectively) with the POTRA domains
860 in the inward-open BamABCDE complex (PDB: 5D0O; light blue) or the outward-open
861 BamACDE complex (PDB: 5EKQ; green). Complexes are superimposed based on 400
862 equivalent C α atoms in the BamA β -barrel, and shown in side (a) or periplasmic (b) view.
863 For 5d0o and 5ekq, the accessory Bam subunits and the BamA β -barrel are omitted for
864 clarity. (c) Periplasmic view of the inward-open BamABCDE complex, showing binding
865 of the BAM accessory proteins BamB (magenta), BamC (red), BamD (blue), and BamE
866 (yellow). Pulldown experiments showed that RcsF binds the BamABCDE complex (Fig.
867 1). In agreement with this observation, structural comparisons reveal that RcsF binding
868 would not result in direct steric clashes with any BAM accessory protein. However, the
869 positions of the POTRA domains in the BamA-RcsF and BamABCDE complexes are
870 markedly different. In the BamA-RcsF complex, POTRA5 makes a 26° outward rotation
871 to accommodate RcsF (see also Fig. 3), and a reorganization in the joint between POTRA
872 domains 3 and 2 results in a more extended conformation of the POTRA “arm” and the
873 projection of POTRA domains 2 and 1 further from the BamA β -barrel, a conformation
874 not previously reported in available BamA structures. In the BamABCDE complex,
875 BamD contacts both POTRA5 and the joint of POTRA domains 1 and 2. In the BamA-
876 RcsF complex, POTRA5 and POTRA domains 2 and 1 are too distant to be bridged by

877 BamD; binding of BamD to BamA-RcsF therefore requires a conformational change in
878 the POTRA arm or the dissociation of BamD at either of these two contact points.

879

880 **Extended Data Figure 4. Validation of the BamA-RcsF structure.** (a) RcsF amino acid
881 sequence. The sequence coverage of the XL-MS experiment was about 60% as
882 highlighted in violet (b) Ribbon diagram of the BamA-RcsF structure. Highlighted
883 residues show sites mutated to amber for incorporation of the photoreactive lysine analog
884 DiZPK. Sites that crosslink to RcsF are green, sites that show no crosslinking are
885 magenta. Mutation of extracellular loop 1 (°L1; red) leads to loss of RcsF binding (see
886 panel g). BamA sidechains found to crosslink with RcsF by means of the
887 homobifunctional amine-reactive crosslinker disuccinimidyl dibutyric urea (DSBU) are
888 shown as sticks and colored cyan. Residue K61 from RcsF, which was found to crosslink
889 to BamA using DSBU, is shown as a stick and colored orange. The other two RcsF
890 residues (K42 and K134) that could be crosslinked to BamA are not visible in this
891 structural model. (c) *In vivo* photocrosslinking experiment in which cells expressing the
892 BamA mutants containing DiZPK at the indicated positions were treated (+) or not (-)
893 with ultraviolet light. Proteins samples were analyzed via SDS-PAGE and immunoblotted
894 with anti-RcsF or anti-BamA antibodies, showing that the photo-crosslinked complexes
895 contain BamA and RcsF. n= 3 biologically independent experiment. WT, wild type. (d,
896 e) Sensorgrams from biolayer interferometry (n=1) (left) and corresponding equilibrium
897 binding plots (right) of immobilized RcsF titrated with BamA (d) or immobilized BamA
898 titrated with RcsF (e). (f) The levels of major OMPs are slightly decreased in cells
899 expressing BamA_{Δloop1}. WT cells harboring the empty plasmid (pAM238) were used as
900 control and EF-Tu expression levels were analyzed as loading control. n= 3 biologically
901 independent experiments. (g) Deletion of loop 1 in BamA prevents RcsF from being

902 pulled down with BamA. WT cells harboring the empty plasmid (pAM238) were used as
903 control. n= 3 biologically independent experiments. **(h)** Overexpression of pBamA Δ Loop1
904 in a *bamA* deletion strain activates the Rcs system compared to WT. A chromosomal
905 *rprA::lacZ* fusion was used to monitor Rcs activity, and specific β -galactosidase activity
906 was measured from cells at mid-log phase (OD₆₀₀=0.5). Boxplot with whiskers (median,
907 first and third percentiles, lower and upper extreme) from minimum to maximum. All
908 values were normalized to the average activity obtained for WT cells harboring the empty
909 plasmid (pET3a) obtained from n= 8 biologically independent experiments. WT, wild
910 type; Kan, kanamycin.

911

912 **Extended Data Figure 5. RcsF binds the inward-open conformation of BamA. (a)**

913 Models for the BamA^{G393C/G584C} 5 and BamA^{G433C/N805C} 26 double cysteine mutants, which
914 are locked in the outward-open or inward-open conformation, respectively, when
915 oxidized. Mutated cysteines are shown as atom spheres. **(b)** BamA barrel locking and
916 RcsF binding. Overexpression of double cysteine mutants pBamA^{G393C/G584C}-B and
917 BamA^{G433C/N805C}-B in a wild-type strain. RcsF can be co-purified with the BamA β -barrel
918 locked in the inward-open conformation (BamA^{G433C/N805C}) by a disulfide bond (ox) but
919 not in the outward-open conformation (BamA^{G393C/G584C}). BamA mutants become
920 reduced (red) following treatment with tris(2-carboxyethyl) phosphine (TCEP) and
921 migrate similarly. The oxidized form of BamA^{G393C/G584C} migrates more slowly than wild-
922 type BamA. As a result, two bands are visible for BamA in the input of BamA^{G393C/G584C},
923 the lower migrating band corresponding to wild-type BamA expressed from the
924 chromosome. n= 3 biologically independent experiments. **(c)** Sensorgram from biolayer
925 interferometry of immobilized RcsF titrated with BamA^{G393C/G584C}, without (oxidized; -
926 DTT) or with dithiothreitol (reduced; + DTT). When the β -barrel is locked in the outward-

927 open conformation (-DTT), RcsF is unable to bind BamA. When reduced,
928 BamA^{G393C/G584C} regains binding, demonstrating that BamA reverts to the inward-open
929 conformation in which it can bind RcsF.

930

931 **Extended Data Figure 6. The movement of POTRA5 towards the periplasmic exit**
932 **of the lumen of the BamA barrel could push RcsF upwards.** (a, b) Lateral view of the
933 initial and final conformations, respectively, of the BamA-RcsF complex during the
934 dynamic importance sampling simulation (DIMS) of the BamA-RcsF complex. (c, d)
935 Bottom view (from the periplasm) of the above conformations. BamA and RcsF are
936 colored in orange and blue, respectively. The initial conformation of the system (BamA
937 and RcsF) corresponds to the structure determined in this work (PDB code 6T1W)⁵ with
938 the POTRA1-4 domains removed. The final conformation of BamA is similar to the
939 outward-open structure (PDB code 5D0Q). The explicit outer membrane and solvent are
940 not shown for clarity. (e) Expression from BamA^{hinge} from a plasmid in Δ *bamA* cells leads
941 to a severe growth defect when cells are grown at 37°C in rich media, but not when they
942 are grown in minimal media at 30°C. Cells were grown in M9 minimal glucose medium
943 at 30°C until they reached OD₆₀₀ =1. Tenfold serial dilutions were made in M9 minimal
944 glucose, plated onto M9 minimal glucose or LB agar, and incubated at 30°C or 37°C.
945 Plates were supplemented with ampicillin (200 µg/ml). n=3 biologically independent
946 experiments.

947 **REFERENCES**

- 948 34 Yu, D. *et al.* An efficient recombination system for chromosome engineering in
949 *Escherichia coli*. *Proc Natl Acad Sci U S A* **97**, 5978-5983,
950 doi:10.1073/pnas.100127597 (2000).
- 951 35 Koskiniemi, S., Pranting, M., Gullberg, E., Nasvall, J. & Andersson, D. I.
952 Activation of cryptic aminoglycoside resistance in *Salmonella enterica*. *Mol*
953 *Microbiol* **80**, 1464-1478, doi:10.1111/j.1365-2958.2011.07657.x (2011).
- 954 36 Roman-Hernandez, G., Peterson, J. H. & Bernstein, H. D. Reconstitution of
955 bacterial autotransporter assembly using purified components. *Elife* **3**, e04234,
956 doi:10.7554/eLife.04234 (2014).
- 957 37 Kabsch, W. Xds. *Acta Crystallogr D Biol Crystallogr* **66**, 125-132,
958 doi:10.1107/S0907444909047337 (2010).
- 959 38 Tickle, I. J., Flensburg, C., Keller, P., Paciorek, W., Sharff, A., Vornrhein, C.,
960 Bricogne, G. . *STARANISO*, 2018).
- 961 39 McCoy, A. J., Grosse-Kunstleve, R.W., Adams, P.D., Winn, M.D., Storoni, L.C.,
962 & Read, R.J. Phaser crystallographic software. *J. Appl. Cryst.* **40**, 658-674 (2007).
- 963 40 Bricogne G., B. E., Brandl M., Flensburg C., Keller P., Paciorek W., & Roversi
964 P, S. A., Smart O.S., Vornrhein C., Womack T.O. BUSTER version 2.10.3.
965 (2017).
- 966 41 Emsley, P. & Cowtan, K. Coot: model-building tools for molecular graphics. *Acta*
967 *Crystallogr D Biol Crystallogr* **60**, 2126-2132, doi:S0907444904019158 [pii]
968 10.1107/S0907444904019158 (2004).
- 969 42 Schmidt, C. & Robinson, C. V. A comparative cross-linking strategy to probe
970 conformational changes in protein complexes. *Nat Protoc* **9**, 2224-2236,
971 doi:10.1038/nprot.2014.144 (2014).

972 43 James, J. M. B., Cryar, A. & Thalassinou, K. Optimization Workflow for the
973 Analysis of Cross-Linked Peptides Using a Quadrupole Time-of-Flight Mass
974 Spectrometer. *Anal Chem* **91**, 1808-1814, doi:10.1021/acs.analchem.8b02319
975 (2019).

976 44 Iacobucci, C. *et al.* A cross-linking/mass spectrometry workflow based on MS-
977 cleavable cross-linkers and the MeroX software for studying protein structures
978 and protein-protein interactions. *Nat Protoc* **13**, 2864-2889, doi:10.1038/s41596-
979 018-0068-8 (2018).

980 45 Osborne, A. R. & Rapoport, T. A. Protein translocation is mediated by oligomers
981 of the SecY complex with one SecY copy forming the channel. *Cell* **129**, 97-110,
982 doi:10.1016/j.cell.2007.02.036 (2007).

983 46 Hussain, S. & Bernstein, H. D. The Bam complex catalyzes efficient insertion of
984 bacterial outer membrane proteins into membrane vesicles of variable lipid
985 composition. *J Biol Chem* **293**, 2959-2973, doi:10.1074/jbc.RA117.000349
986 (2018).

987 47 Miller, J. C. *Experiments in Molecular Genetics*. (Cold Spring Harbor Laboratory
988 Press, 1972).

989 48 Sali, A. & Blundell, T. L. Comparative protein modelling by satisfaction of spatial
990 restraints. *J Mol Biol* **234**, 779-815, doi:10.1006/jmbi.1993.1626 (1993).

991 49 Lomize, M. A., Pogozheva, I. D., Joo, H., Mosberg, H. I. & Lomize, A. L. OPM
992 database and PPM web server: resources for positioning of proteins in
993 membranes. *Nucleic Acids Res* **40**, D370-376, doi:10.1093/nar/gkr703 (2012).

994 50 Lee, J. *et al.* CHARMM-GUI Membrane Builder for Complex Biological
995 Membrane Simulations with Glycolipids and Lipoglycans. *J Chem Theory*
996 *Comput* **15**, 775-786, doi:10.1021/acs.jctc.8b01066 (2019).

997 51 Wu, E. L. *et al.* E. coli outer membrane and interactions with OmpLA. *Biophys J*
998 **106**, 2493-2502, doi:10.1016/j.bpj.2014.04.024 (2014).

999 52 Fleming, P. J. *et al.* BamA POTRA Domain Interacts with a Native Lipid
1000 Membrane Surface. *Biophys J* **110**, 2698-2709, doi:10.1016/j.bpj.2016.05.010
1001 (2016).

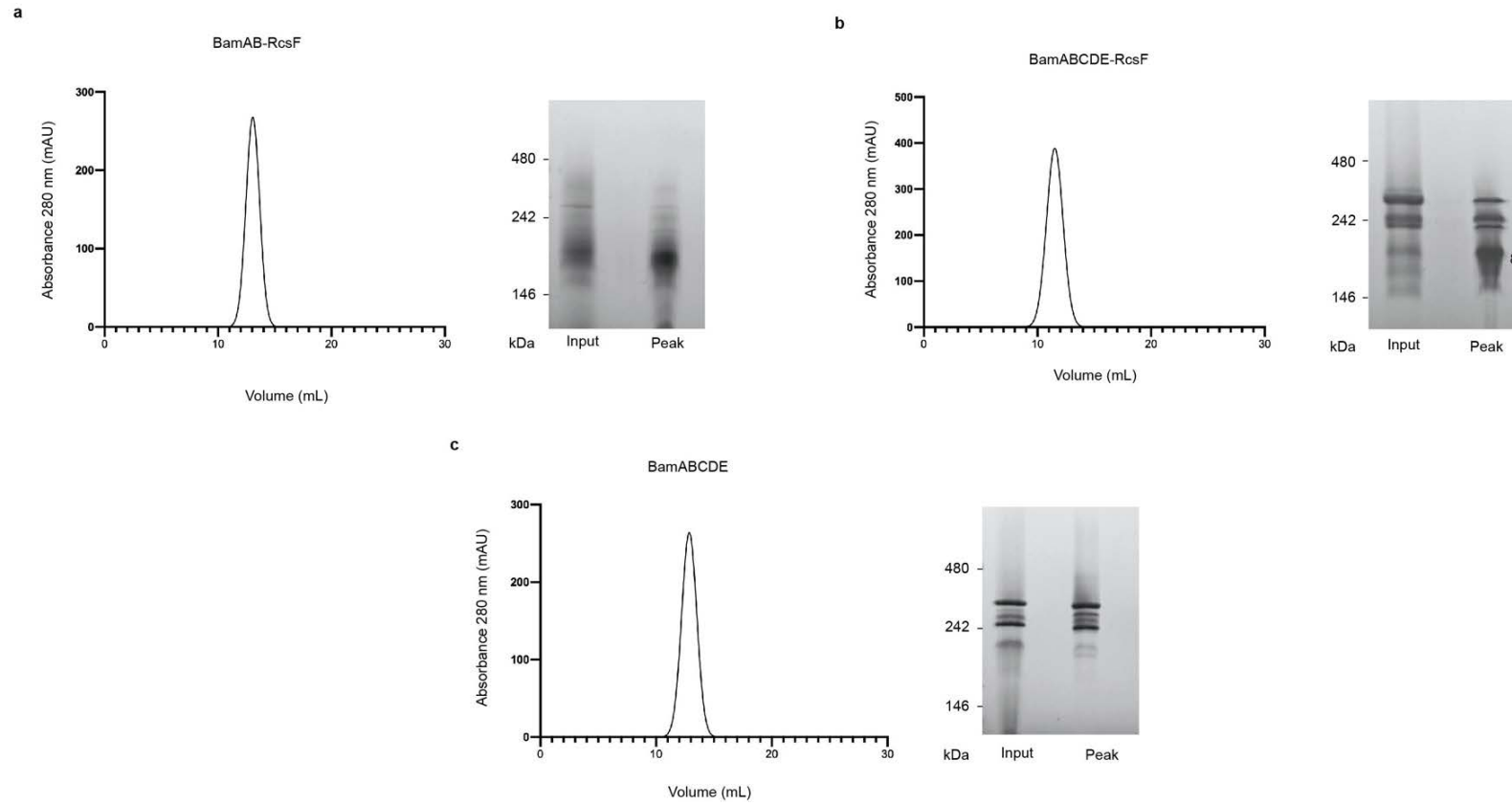
1002 53 Brooks, B. R. *et al.* CHARMM: the biomolecular simulation program. *J Comput*
1003 *Chem* **30**, 1545-1614, doi:10.1002/jcc.21287 (2009).

1004 54 Perilla, J. R., Beckstein, O., Denning, E. J. & Woolf, T. B. Computing ensembles
1005 of transitions from stable states: Dynamic importance sampling. *J Comput Chem*
1006 **32**, 196-209, doi:10.1002/jcc.21564 (2011).

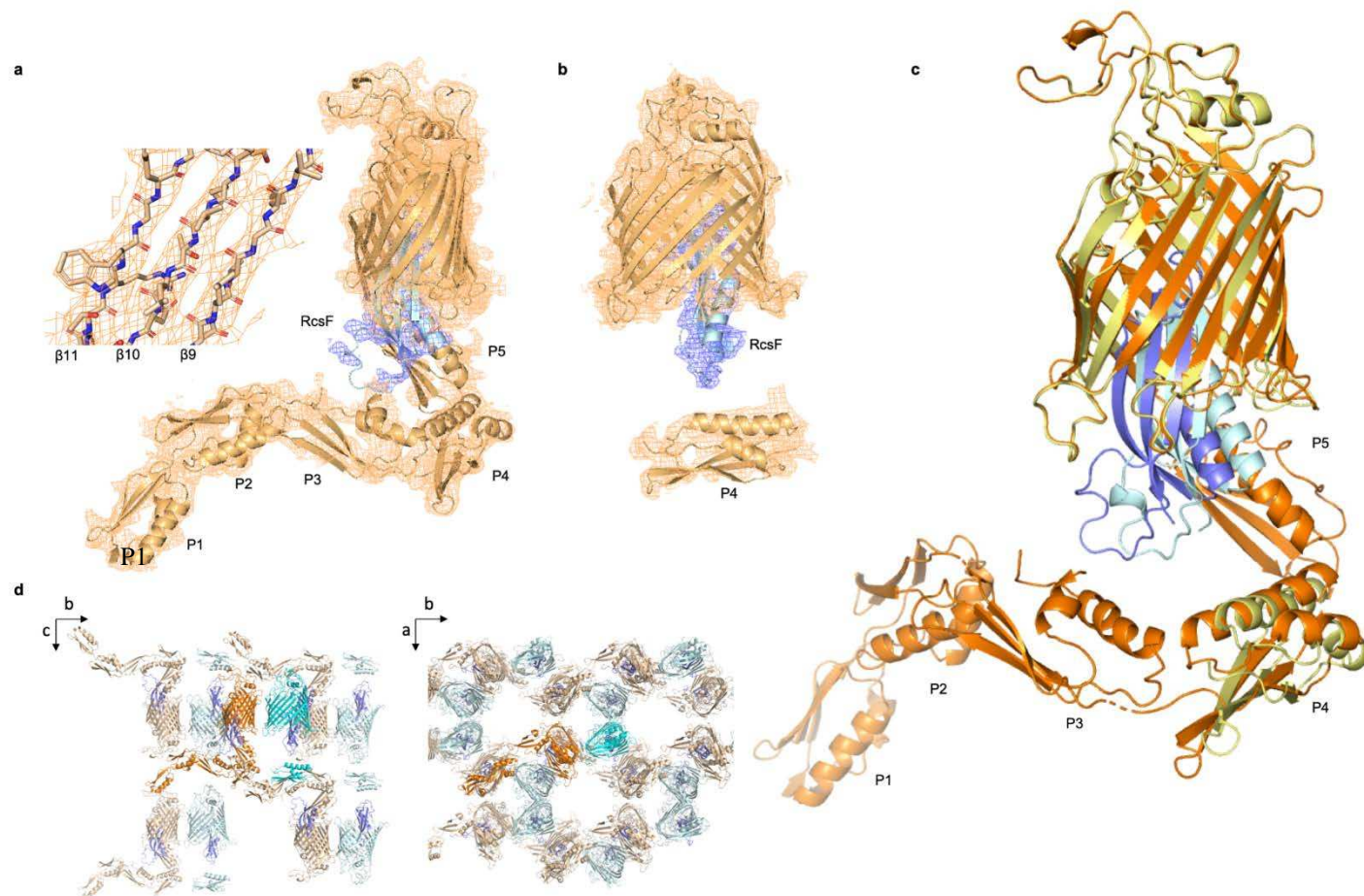
1007 55 Denning, E. J. & Woolf, T. B. Cooperative nature of gating transitions in K(+)
1008 channels as seen from dynamic importance sampling calculations. *Proteins* **78**,
1009 1105-1119, doi:10.1002/prot.22632 (2010).

1010 56 Humphrey, W., Dalke, A. & Schulten, K. VMD: visual molecular dynamics. *J*
1011 *Mol Graph* **14**, 33-38, 27-38, doi:10.1016/0263-7855(96)00018-5 (1996).

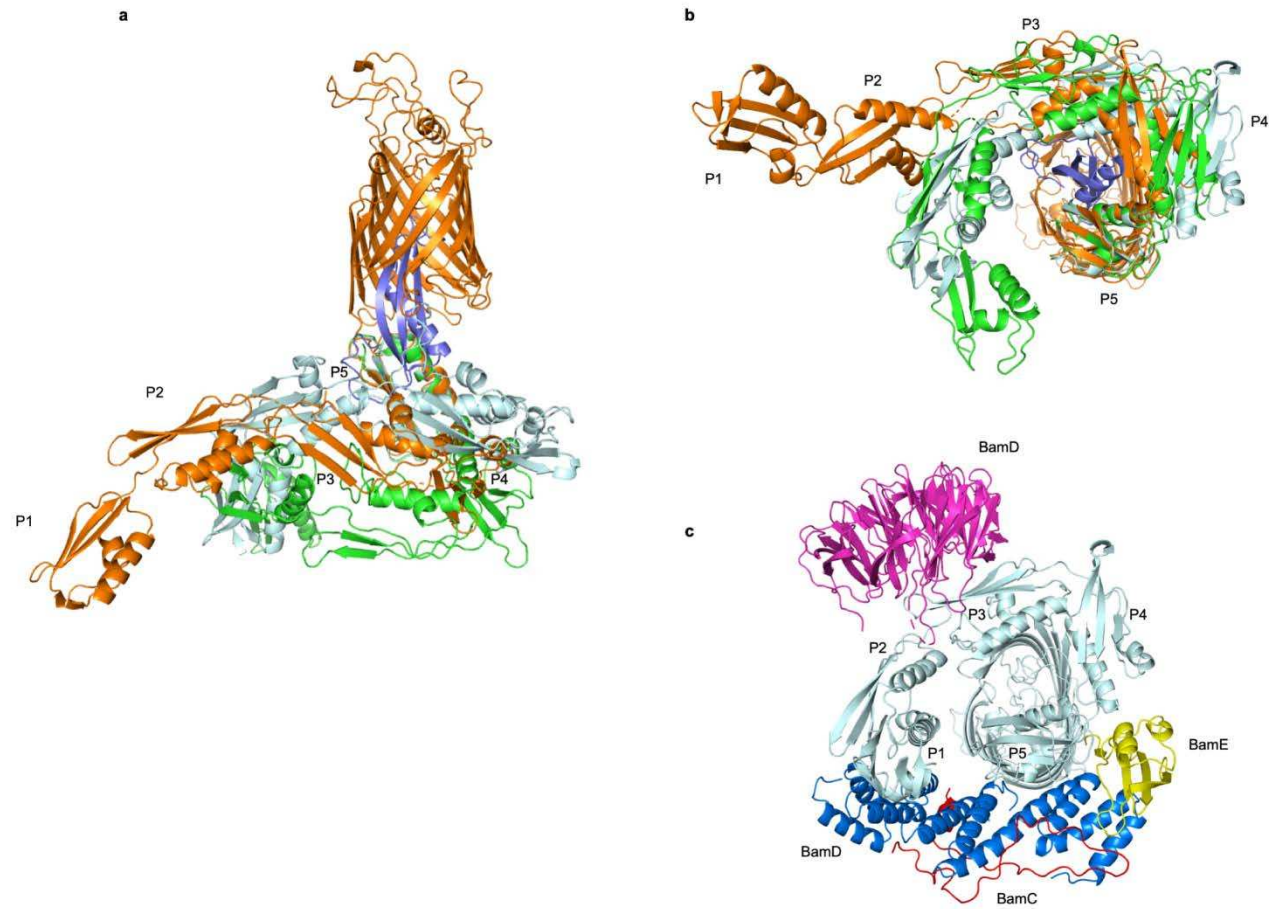
Extended Data Figure 1



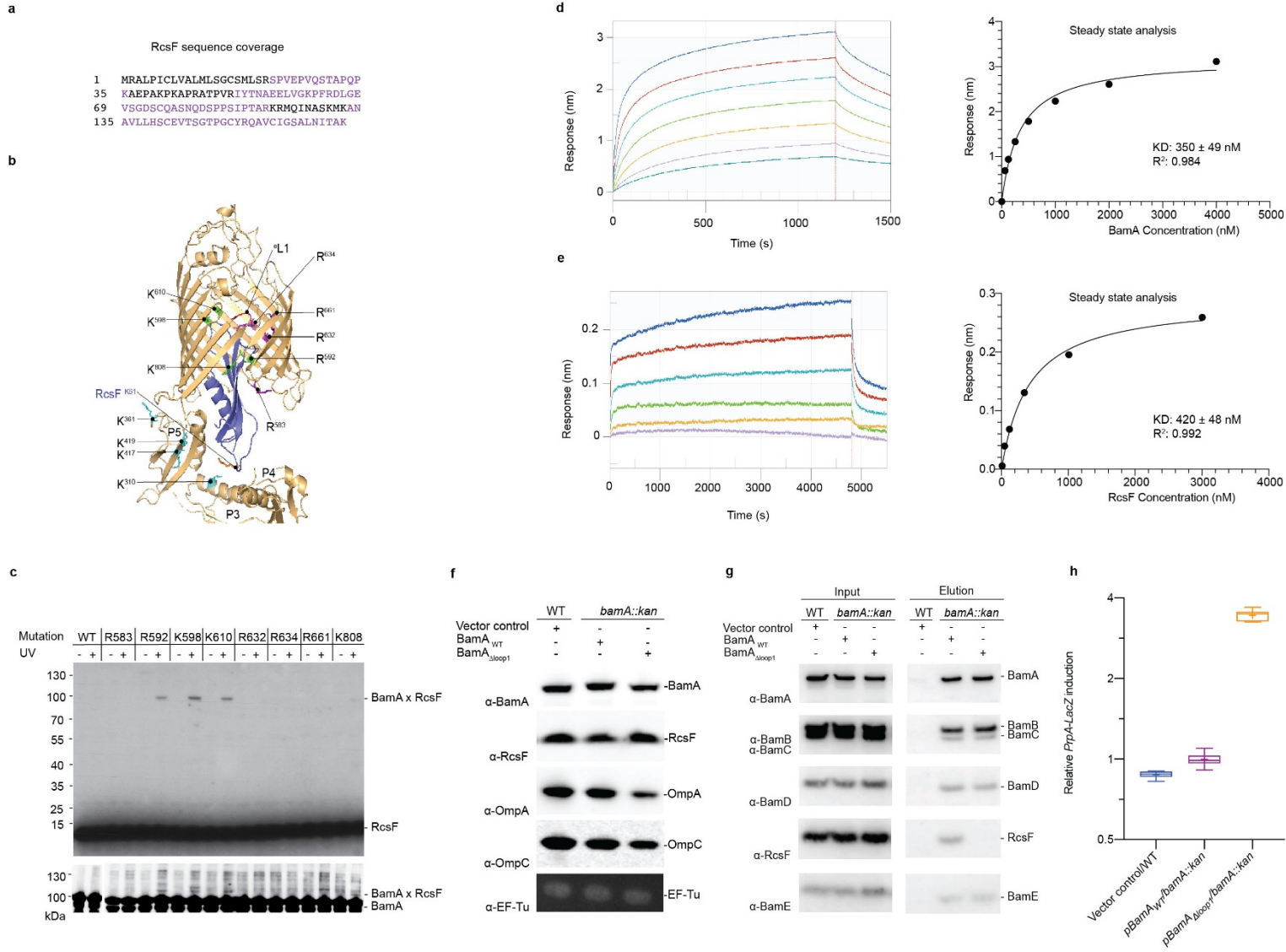
Extended Data Figure 2



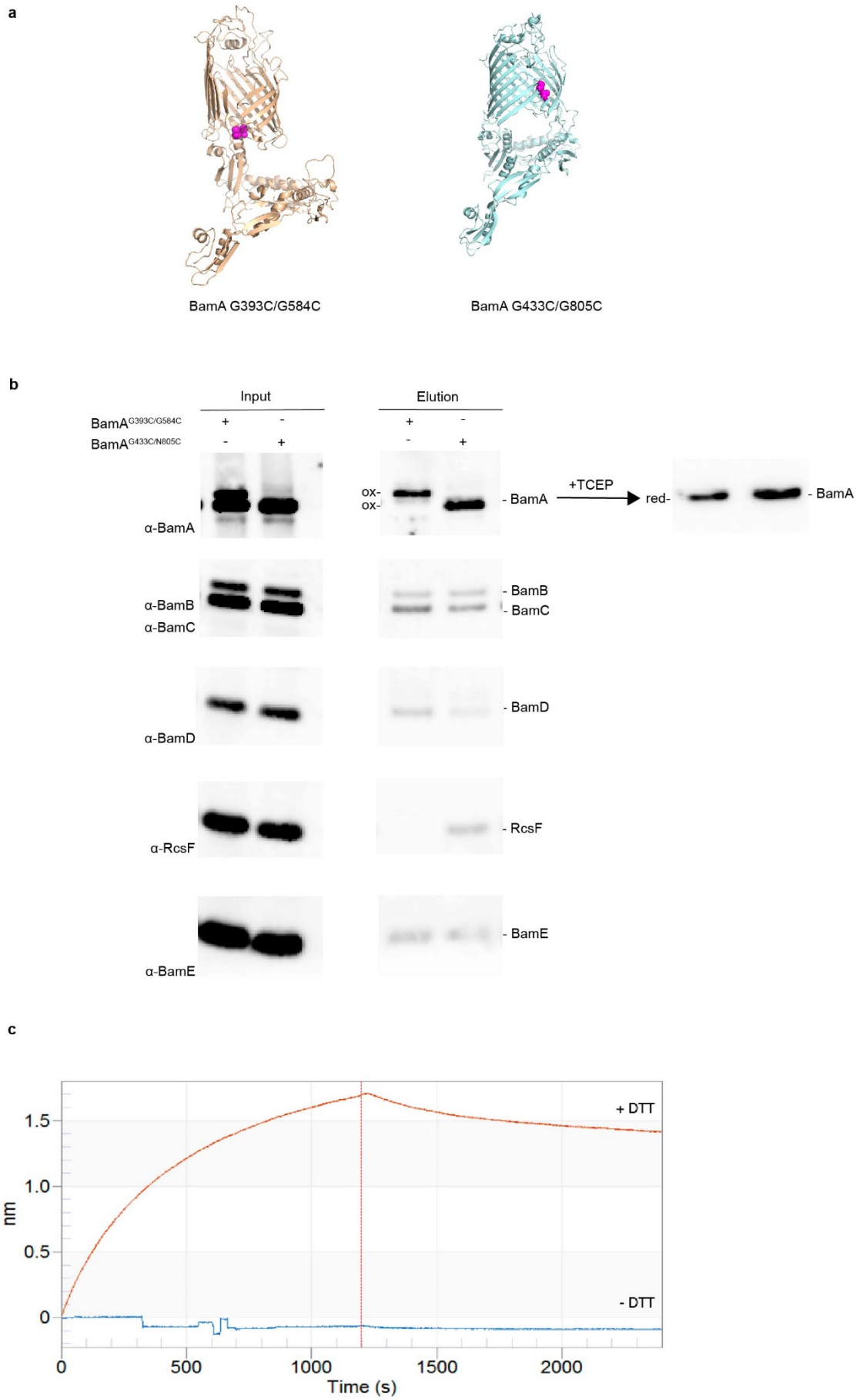
Extended Data Figure 3



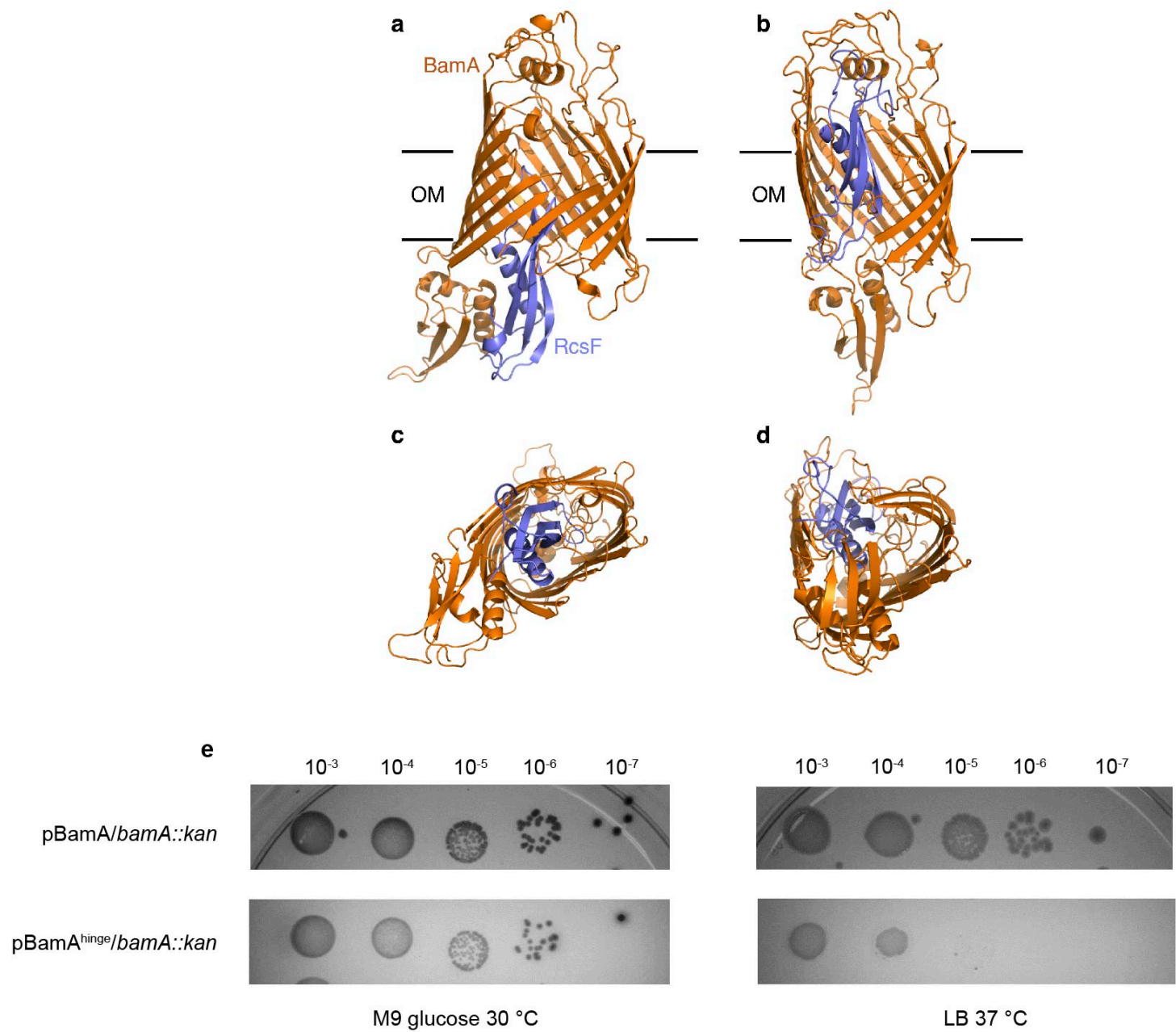
Extended Data Figure 4



Extended Data Figure 5



Extended Data Figure 6



Supplementary Information

Supplementary Table 1. Data collection and refinement statistics.

BamA-RcsF	
Data collection	
Space group	C2
Cell dimensions	
<i>a</i> , <i>b</i> , <i>c</i> (Å)	158.84, 142.53, 116.42
α , β , γ (°)	90.0, 102.6, 90.0
Resolution (Å)**	48.6 – 3.8 (4.0 – 3.8) *
<i>R</i> _{pim}	0.02 (0.79)
<i>I</i> / σ <i>I</i>	15.9 (0.8)
Completeness (%)	
Spherical	71.2 (24.9)
Elliptical**	92.8 (91.4)
Redundancy	34.3 (31.7)
Wilson B (Å ²)	149.4
Refinement	
Resolution (Å)	48.6 – 3.8
No. reflections	18489
<i>R</i> _{work} / <i>R</i> _{free}	28.1 / 31.7
No. atoms	
Protein	10838
Ligand/ion	NA
Water	NA
<i>B</i> -factors (Å ²)	
Protein	193.5
Ligand/ion	NA
Water	NA
R.m.s. deviations	
Bond lengths (Å)	0.01
Bond angles (°)	1.15

*Values in parentheses are for highest-resolution shell.

** Elliptical diffraction limits and principal reciprocal axes of the fitted ellipsoid: 4.6 Å along 0.987 a* - 0.158 c*, 4.4 Å along b* and 3.8 Å along c*

Supplementary Table 2. Intermolecular BamA-RcsF crosslinks detected.

PSMs = Peptide Spectrum Matches. The POTRA domain in BamA where the crosslinked residue is located is also indicated.

BamA Residue	RcsF Residue	BamA Peptide			RcsF Peptide			PSMs	POTRA
		Sequence	Start	End	Sequence	Start	End		
310	61	K LLGR	310	314	IYTNAEELVG K PFR	51	64	3	4
361	42	FEGND T SKDAVLR	354	366	AEP A K P KAPR	36	45	3	5
361	61	FEGND T SKDAVLR	354	366	IYTNAEELVG K PFR	51	64	78	5
310	134	K LLGR	310	314	QAVCIGSALN I TAK	121	134	1	4
417	61	VPGSPDQVDV V Y K VK	405	419	IYTNAEELVG K PFR	51	64	14	5
419	61	V KER	418	421	IYTNAEELVG K PFR	51	64	24	5

N.B. Residue 134 is the C-terminal Lys of RscF

Supplementary Table 3. Strains used in this study.

Strains	Genotype and description	Source
BL21 (DE3)	<i>F- ompT hsdSB (rB- mB-) gal dcm</i> (DE3)	Novagen
DH300	<i>rprA-lacZ</i> MG1655 (<i>argF-lac</i>) <i>U169</i>	32
PL339	Δ <i>rcsF::kan</i>	10
PL358	DH300 Δ <i>rcsF</i>	10
Keio collection single mutants	Δ <i>rcsF::kan</i>	33
RRA73	BL21 (DE3) with pRRA1	This study
RRA74	BL21 (DE3) with pRRA1 and pSC216	This study
SEN1071	PL358 with pJH118 and pSC216	This study
SEN1472	DH300 Δ <i>bamA::kan</i> with pSC270	This study
SEN1603	DH300 Δ <i>bamA::kan</i> with pBamA	This study
SEN1607	DH300 Δ <i>bamA::kan</i> with pBamA Δ loop1	This study
SEN1411	DH300 with pET3a and pAM238	This study
SEN991	DH300 with pBamA and pAM238	This study
SEN1597	DH300 with pBamA-B and pAM238	This study
SEN1598	DH300 with pBamA-B and pSC263	This study
RRA54	DH300 with pBamA ^{G393C/G584C} -B and pAM238	This study
RRA106	DH300 with pBamA ^{G433C/N805C} -B and pAM238	This study
SEN1723	DH300 Δ <i>bamA::kan</i> with pBamA ^{hinge}	This study

1

Supplementary Table 4. Plasmids used in this study.

Plasmids	Features	Source
pAM238	IPTG-regulated Plac, pSC101-based, spectinomycin	⁵⁷
pBAD33	Arabinose regulation, pACYC184-based, chloramphenicol	⁵⁸
pSC231	pAM238 with LacI ^q and the modified P _{trc}	¹⁰
pSIM5-tet	pSC101-based, <i>repA^{ts}</i> , tetracycline	³⁵
pSUPAR-Mb-Dizpk-RS	PyIRS, tRNA ^{PyI} _{CUA} opt, p15A origin, chloramphenicol	²⁴
pET3a	T7 promoter, ampicillin	Novagen
pTrc99a	IPTG-regulated P _{trc} , ampicillin	⁵⁹
pBamA	pET23a with BamAss-6xHis-2xAla-BamA(E22-W810), Ampicillin	¹⁰
pBamA ^{hinge}	pBamA (BamA with the insertion of a LVPR sequence at position 424)	This study
pBamA _{Δloop1}	pBamA (BamA with the deletion from T434-G437)	This study
pBamA-B	pBamA::BamB	This study
pBamA ^{G393C/G584C} -B	pBamA _{L6} -B with BamA ^{G393C/G584C}	This study
pBamA ^{G433C/N805C} -B	pBamA _{L6} -B with BamA ^{G433C/N805C}	This study
pSC263	pAM238 with BamCDE, spectomycin	This Study
pSC216	pBAD33 with RcsF	¹⁰
pJH114	pTrc99a::BamA-BamB-BamC-BamD-BamE-6xHis	³⁶
pJH118	pTrc99a::6xHis-BamA-BamB	³⁶
pRRA1	pJH114 but with modifications: 6xHis-BamA and BamE with no 6xHis	This study
pSC270	pSC231 with BamA	This study
pSC270 ^{R583X}	amber codon (TAG) replacing the codon for the designated amino acid residues	This study
pSC270 ^{R592X}	amber codon (TAG) replacing the codon for the designated amino acid residues	This study
pSC270 ^{R598X}	amber codon (TAG) replacing the codon for the designated amino acid residues	This study
pSC270 ^{R610X}	amber codon (TAG) replacing the codon for the designated amino acid residues	This study
pSC270 ^{R632X}	amber codon (TAG) replacing the codon for the designated amino acid residues	This study

pSC270 ^{R634X}	amber codon (TAG) replacing the codon for the designated amino acid residues	This study
pSC270 ^{R661X}	amber codon (TAG) replacing the codon for the designated amino acid residues	This study
pSC270 ^{K808X}	amber codon (TAG) replacing the codon for the designated amino acid residues	This study

Supplementary Table 5. Primers used in this study.

Name	Sequence (5' to 3')
bamB (NotI) R	GAGAGCGGCCGCTTAACGTGTAATAGAG
pTrc-for	CAAGGCGCACTCCCGTTCTGG
pTrc-rev2	CGCCAGGCAAATTCTG
BamA (PciI)F	GAGACATGTTGGCGATGAAAAAGTTGC
BamA (XbaI)R	GAGTCTAGATTACCAGGTTTTACCG
bamC kpnI F	GATCGGTACCTCGGATCTTAGGGAGATTTGATGGC
bamA Km del F	GATTTCTCTCGGTTATGAGAGTTAGTTAGGAAGAACG CATAATAACGATGATTCCGGGGATCCGTCGACC
bamA Km del R	CTACCACTACATTCCTTTGTGGAGAACACTTACCAGG TTTTACCGATGTTTGTAGGCTGGAGCTGCTTCG
SDM-His-BamA F	CACCATCACCACCATGGCGCGGCCGAAGGGTTCGTA GTGAAAGATATTCATTTG
SDM-His-BamA R	CGCCATGGTGGTGATGGTGATGGGCCGCGTATACGG TGGCG
bamE delHis F	TGCGCTGAGTGGTAACTAAGATCCTCTAGAGTCGAC
bamE delHis R	GTCGACTCTAGAGGATCTTAGTTACCACTCAGCGCA
BamA Hinge F	GTAAAAGAGCGCAACACCCTGGTGCCGCGCGGTAGC TTCAACTTTGGT
BamA Hinge R	ACCAAAGTTGAAGCTACCGCGCGGCACCAGGGTGTT GCGCTCTTTTAC

3 **Supplementary Video**

4 **Dynamic importance sampling (DIMS) simulation of the BamA-RcsF complex**

5 **reproducing the proposed push-and-pull model.** The simulation shows the transition

6 of BamA from the inward-open to the outward-open conformation, with the POTRA5

7 domain moving towards the periplasmic exit of the lumen and pushing RcsF upwards.

8 This movement is accompanied later on by the movement of strands 1-6 in BamA (Z1

9 domain) and the opening of the outward-facing extremity. The initial conformation of the

10 system (BamA and RcsF) corresponds to the inward-open structure determined in this

11 work (PDB code 6T1W) with the POTRA1-4 domains removed. The final conformation

12 of BamA is similar to the outward-open structure (PDB code 5D0Q). The proteins are

13 represented as cartoons (BamA and RcsF colored in orange and blue, respectively), the

14 explicit outer membrane represented as sticks and the oxygen atoms of water molecules

15 represented as red dots.

16